Journal of Industrial and Engineering Chemistry 85 (2020) 34–65

Contents lists available at ScienceDirect

Journal of Industrial and Engineering Chemistry

journal homepage: www.elsevier.com/locate/jiec

Advanced ceramic components: Materials, fabrication, and applications

Tunmise Ayode Otitoju[a], Patrick Ugochukwu Okoye[b], Guanting Chen[d], Yang Li[a], Martin Onyeka Okoye[c], Sanxi Li[d,*]

[a] School of Materials Science and Engineering, Shenyang University of Technology, Shenyang 110870, China
[b] Laboratorio de Bioenergía, Instituto de Energías Renovables (IER-UNAM), Temixco, Morelos 62580, Mexico
[c] School of Electrical Engineering, Shenyang University of Technology, Shenyang 110870, China
[d] School of Science, Shenyang University of Technology, Shenyang 110870, China

ARTICLE INFO

Article history:
Received 26 November 2019
Received in revised form 23 January 2020
Accepted 4 February 2020
Available online 8 February 2020

Keywords:
Ceramics
Ceramic components
Properties
Fabrication
Applications

ABSTRACT

The global demand for ceramic materials with wide-ranging applications in the environment, precision tools, biomedical, and electronics, and environmental fields is on the increase. Several ceramic materials and methods of fabrication have been developed with task-specific properties. The material, the fabrication methods, and processing conditions impel characteristics including corrosion-resistant, outstanding optical and electrical properties, hardness and anti-aging. In this review, various materials for the preparation of ceramics and ceramic composites components were investigated to demonstrate the contribution of the materials and different fabrication methods to the properties of the ceramics components. The material properties, sintering temperature, casting technique, and pressure influences the ceramics grain size and porosity, which have an explicit effect on mechanical strength, corrosion-resistant, and optical properties of the ceramic components. The finishing of the ceramic components into a machinable shape requires careful attention to avoid defects. However, most conventional finishing methods are cost-intensive, hence, the need to commercialize 3-D printing for large scale and long-run applications. It is hoped that this review would propagate wider research on low cost and energy effective pathways to produce ceramics with dynamic properties, which can be applied in several fields with outstanding performance.

Abbreviations: abs., absolute, Al_2O_3 Alumina; AMC, alumina matrix composites; AlN, aluminum nitride; AlON, aluminum oxynitride; AMPG, O-(2-aminopropyl)-O′-2-methoxyethyl-polypropyleneglycol; APTES, 3-aminopropyltriethoxysilane; ATZ, alumina-toughened zirconia; aq, aqueous; BBP, butyl benzyl phthalate; BLZT, $0.07Ba_{0.94}La_{0.04}Zr_{0.02}Ti_{0.98}O_3$; BN, boron nitride; BNT, $0.93Bi_{0.5}Na_{0.5}TiO_3$; CaO, calcia; CeO_2, ceria; CIP, cold isostatic pressing; CR, cooling rate; CTAB, cetyl trimethyl ammonium bromide; CTE, coefficient of thermal expansion; CuO, copper(II) oxide; CVD, chemical vapor deposition; DBP, dibutyl phthalate; DI, deionized; DRA, dielectric resonator antenna; β-eucryptite, β-$LiAlSiO_4$; FAS, 1H, 1H, 2H, 2H-perfluorooctyltriethoxysilane; GDC, Gd_2O_3 and CeO_2; HAP, hydroxyapatite; HAPES, high alkane phase emulsified suspensions; HDPE, high density polyethylene; HF, hollow fiber; HFM, hollow fiber membrane; HPSN, hot pressed silicon nitride; HR, heating rate; HTCC, high temperature co-fired ceramic; ID, inner diameter; IP, interfacial polymerization; KOH, potassium hydroxide; LTCC, low temperature co-fired ceramics; Mg, magnesium; MgO, magnesium oxide; NA, not available or not applicable; NaPAA, sodium polyacrylate; NiO-GDC, $(NiO)_{30}$-$(GDC)_{70}$; NIPs, non-solvent induced phase separation; NMP, *N*-methyl-2-pyrrolidone; NP, nanoparticle; NRA, nanorod arrays; OD, outer diameter; PAA, polyacrylic acid; PEG, polyethylene glycol; PES, polyethersulfone; PFOA, perfluorooctanoate; PFOS, perfluorooctanesulfonate; PIM, powder injection molding; PSD, particle size distribution; PSZ, partially stabilized zirconia; PU, polyurethane; PVB, polyvinyl butyral; PVP, polyvinylpyrrolidone; PWF, pure water flux; RH, relative humidity; RT, room temperature; SCS, solution combustion synthesis; SFF, solid freeform fabrication; SHS, self-propagating high-temperature synthesis; Si, silicon; SiAlON, silicon aluminum oxynitride; SiBCO, silicon boron oxycarbide; Si_3N_4, silicon nitride; SiC, silicon carbide; SICO, silicon oxycarbide; SiO_2, silicon dioxide; β-Sialon, $Si_{6-z}Al_zO_zN_{8-z}$; SLS, sodium lauryl sulphate; STL, $SrTiO_3$+0.5 wt% Li_2CO_3; STL/BNT-BLZT, $SrTiO_3$+0.5 wt.% Li_2CO_3)/($0.93Bi_{0.5}Na_{0.5}TiO_3$-$0.07Ba_{0.94}La_{0.04}Zr_{0.02}Ti_{0.98}O_3$; TEM, transmission electron microscopy; THF, tetrahydrofuran; TiB_2, titanium diboride; TiC, titanium carbide; TiCN, titanium carbonitride; TIF, temperature-induced forming; TiO_2, titanium dioxide; Ti_3SiC_2, titanium silicocarbide; TZP, tetragonal ZrO_2 polycrystal; UDP, uniaxial die pressing; UHTCs, ultra-high temperature ceramics; ULTCC, ultra-low temperature co-fired ceramics; VFD, vacuum freeze drying; WC, tungsten carbide; Y_2O_3, yttria; Y-TZP, Y_2O_3-stabilized zirconia; 3Y-TZP, 3 mol% yttria-stabilized ZrO_2; ZrB_2, zirconium diboride; ZrC, zirconium carbide; ZrO_2, zirconia; $ZrSiO_4$, zirconium orthosilicate or zirconium silicate; ZTA, zirconia-toughened alumina; ZTE, zero coefficient of thermal expansion; 3-D, three dimension.

* Corresponding author.
E-mail address: lisx@sut.edu.cn (S. Li).

https://doi.org/10.1016/j.jiec.2020.02.002
1226-086X/

Contents

Introduction

The term ceramics comes from the Greek word “Keramicos” which basically means burnt materials. They are known for over a thousand centuries and are prepared from naturally occurring raw materials. Ceramics are normally inorganic and non-metallic solids (prepared from powdered materials), having relatively melting points and requires high temperature for their processing and applications. They are usually a compound of different elements or a combination of compounds, between metallic and non-metallic elements (mainly O, B, C, N), which can be oxides, carbides, borides, silicides. Their bonds are either totally ionic or the combination of covalent and ionic. Ceramics as compared to other materials present vast interesting properties including thermal insulation, lightness, high specific surface area and thermal shock resistance. Usually, ceramics do not deform at the long-operation cycle, facilitating lower cost of maintenance [1] and have excellent stability in a variety of organic solvents. They do not cause toxic effects in the marine environment because of facile tailoring of their pore structure, and chemical inertness [2]. There are two types of ceramics namely traditional and advanced ceramics. The former is made up of inorganic non-metallic solid (either non-metallic or metallic compounds) and includes clay (plastic materials), silica (filler) and feldspar (fluxes) while the latter is made up of oxides, nitrate compounds, carbides and non-silicate glass. Traditionally, ceramics are commonly oxide compositions are produced in both amorphous and crystalline states. In many forms, they are not fully dense and contain porosity at the micro and higher size range [3]. In traditional ceramics, clay confers hardness and ductility, silica determines high stability at elevated melting point and high temperature, and feldspar produces the glass phase when the ceramics are fired. Some examples of traditional ceramics include tiles, glasses, porcelain and bricks. Table 1 presents the advantages and disadvantages of traditional and advanced ceramics. Advanced ceramics are different from traditional ceramics by their higher strength, tailorable properties, improved toughness, higher operating temperatures and these characteristics make up modern ceramic components. The scope of this review only covers one aspect of ceramics which is the advanced ceramics. The trends and research effort on the advanced ceramics components formulation, fabrication, and applications are presented.

Advanced ceramic materials

Advanced ceramics can also be referred to as the high-performance ceramics, high-tech ceramics, engineering ceramics, fine ceramics, and technical ceramics. They are basically crystalline material of rigorously controlled composition and manufactured with detailed regulation from highly refined or/and characterized raw materials that give precisely specified attributes. Current ceramic materials may be oxides, carbides, nitrides, silicides, borides, etc. Table 2 presents a list and properties of relevant advanced ceramics. Some values provided were compiled from peer-reviewed literatures and are considered not material specifications. However, the values are considerably equivalent for ceramic materials used in various applications. These properties are specific to individual ceramic material and cannot directly be compared. Although, they may play vital roles during the applications and performance of ceramic components.

Preparation of advanced ceramic materials

The preparation of advanced ceramic components involves the heating process of ceramic powders, which must undergo special handling to control the heterogeneity, chemical compositions, purity, particle size, particle size distribution (PSD) and specific shape. The aforementioned factors play a significant role in the properties of finished ceramic components. Theoretically, it is very possible to distinguish between finished ceramic components obtained from naturally harvested materials and materials prepared from fully synthetically. Most binary oxide ceramics like SiO_2 or Al_2O_3 can be processed from non-oxide ceramics while natural sources, as well as more-complex oxides like high

Table 1
Advantages and disadvantages of traditional and advanced ceramics.

	Traditional ceramics	Advanced ceramics
Raw materials	Are made from natural minerals without processing, such as clay, feldspar, quartz.	Are made from synthetic high-quality powders. These selected raw materials are responsible for the provision of special functions and qualities.
Structures	The structures are decided by the composition of the clay. For instance, ceramics from different origins have various textures. Because of the use of different raw materials, traditional ceramics tend to have more complicated chemical structures and compositions. Besides, traditional ceramic has more impurities both in quantity and type. The microstructure of traditional ceramics is not even with multiple pores. Therefore, it is harder to control the quality of traditional ceramic products.	The chemical structures of advanced ceramics are clear and simple with high purity. Moreover, they are made from manually calculated ingredients, which means the raw materials are under control. Therefore, the microstructure of advanced ceramics is generally fine and uniform.
Manufacturing processes	The minerals for traditional ceramics can be directly used for wet moldings, including grouting molding of the slurry or plastic molding of mud. The green body requires no further processing after sintering with the temperature between 900 to 1400 °C.	Dry molding and wet molding can only be suitable for advanced ceramics when organic additions are added to the raw materials of high-purity powders. There is still a need for further processing after firing under a higher sintering temperature, from 1200 to 2200 °C according to different materials. From the perspective of preparation procedures, advanced ceramics overcome the limits of traditional ceramics. Moreover, there are many advanced technologies used in precise ceramics including hot and high-temperature isostatic pressing, protective atmosphere sintering, vacuum sintering, hot pressing, etc.
Functions and applications	Traditional ceramic materials are mainly produced for daily work or use as building materials.	Advanced ceramics have better performances in quality as well as new applications that traditional ones don't have. They have multiple physical and mechanical properties including high hardness, high strength, thermal shock resistance, wear resistance, corrosion resistance, and high-temperature resistance. They also have great potential for use in sound, magnetism, heat, electricity, light, biology, chemistry, and other applications.

temperature superconductors, can be obtained via complex synthetic routes.

The most widely used processes such as the solid-state reactions are suitable for the mass-production of cost-effective ceramic powders. Highly pure ultra-fine powders are synthesized by using gas-phase reactions. Liquid phase synthesis for the production of homogeneous fine powders involves the hydrothermal synthesis and a coprecipitation method. The main reaction controlling parameter in most synthesis routes being temperature. Together with temperature, pressure has also been used in recent approaches for the synthesis of novel ceramic nitrides including γ-Si_3N_4 or cubic Hf_3N_4 and Zr_3N_4. For some high-pressure ceramic synthesis studies, laser-heated diamond anvil cell techniques and multi-anvil techniques have also been successfully applied [4,5]. Carbothermal reduction is practiced commercially for the synthesis of many non-oxide powders such as borides, carbides, and nitrides. Carbothermic reduction of Al_2O_3 has the potential for lower capital investment, much greater production per unit, a cheaper ore and less consumption of electric power. The term self-propagating high temperature synthesis is presently being used to describe a process in which initial reagents, when ignited, spontaneously transform into products, due to the exothermic heat reaction. Several other terminologies such as gasless combustion, combustion synthesis, self-propagating combustion, self-propagating exothermic reactions are used to describe the same process [6]. This process which is an offshoot of pyrotechnics evolved from the studies that were carried out on the combustion of solid cylindrical compacts like Ti-B mixtures by Merzhanov et al. [7]. The combustion reduction is initiated at one point and then propagates rapidly via reaction mixture in the form of a combustion wave. In this process, the heat of reaction furnishes more than 90 % of the energy required for the synthesis.

More recently methods including polymer pyrolysis, the sol-gel technique and chemical vapor deposition (CVD) have also been introduced to create high-purity ceramic materials with well-defined properties. In CVD, a lower molecular and volatile reactant in the gas phase are fed into a hot reaction zone in which a solid reaction product is obtained and collected as a free powder (thermo-dynamic instability of gaseous reactants being the driving force). The total deposition rate is dependent on the diffusion rate, nucleation rate, and reaction rate. Diffusion and reaction are the rate-determining factors at a higher and lower temperature, respectively. The formation of free powders in the reactor atmosphere is as a result of homogeneous nucleation. The sol-gel process involves the manufacture of oxide ceramics through the peptization of metal oxides or hydrolysis of metal salts with subsequent coagulation of colloidal gels. Additionally, it may also involve hydrolysis of alcoholic solutions of metal alkoxides, acetylacetonates or acetates forming polymeric gels, and formates. The colloidal gels formation is preceded by the sol formation (particle size of 0.01 to 0.1 mm), whereby the suspended colloidal particles are in either steric interaction or electrostatic by means of polymer or surface-active substances. Upon sols destabilization, for example, by removal of the liquid-phase or change in pH value, the particles of the sol coagulate to form a 3D gel [8]. During the drying process (determines the formation of defect-free gels), considerable capillary forces come into play and these forces increase with a decrease in capillary radius. In addition, these processes can open new application areas that are previously not achievable by conventional methods. Among the mentioned processes, the ceramic solid is synthesized based on the lower-molecular, elemental organic or inorganic precursors. The two major advantages of using heavily milled ceramics that are produced via the sol-gel approach include the reduced cost of sintering and reduction of grain size.

Fabrications of ceramic components

The fabrication of ceramic components can be achieved via several techniques. In general, ceramic components can be configured in a variety of geometries including hollow fibers, tubes, and flat discs. Furthermore, ceramic components can be processed in four different stages such as material preparation, processing, sintering and finishing. There are varieties of methods involved to process ceramics components including dry forming, wet forming, gel-casting, thixotropic casting, direct foaming,

Table 2
Advanced ceramic materials, structural phases, and properties.

Ceramic materials	Phases/Bonds/Forms	Properties
Aluminum oxide (Al_2O_3)	Its microstructure mainly includes covalent bonds or ionic bonding. It exists in three phases (α phase, β-phase and γ-Al_2O_3).	Density (3950 kg/m^3), flexural strength (~379 MPa), elastic modulus (375 GPa), compressive strength (~2600 MPa), hardness (1440 kg/mm^2), fracture toughness (4 MPa m $^{1/2}$), thermal conductivity (35 W/m K), CTE (8.4×10^{-6} °C^{-1}), dielectric constant (9.8 at 1 MHz), low cost, relative abundance and are environmentally friendly.
Aluminum nitride (AlN)	Possesses hexagonal crystal structure and is covalently bonded.	Chemical stability, band gap (6.2 eV, direct), hardness (1100 kg/mm^2), critical electric field (~12 MV/cm) and oxidation resistance, thermal conductivity (~320 W/m K) and static dielectric constant (8.5–8.8 at 1 MHz), binding energy of 11.52 eV/atom, compressive strength (2100 MPa), elastic modulus (~330 GPa), fracture toughness (2.6 MPa m $^{1/2}$), CTE (4.2–5.8×10^{-6} °C^{-1}), relatively high piezoelectric constants (d_{33} = 3.4 pm/V, e_{31} = 1.0 C/m^2) and dielectric permittivity (10.4), good semiconductor process compatibility, dielectric consumption (≈4×10^4), non-toxic, density (3260 kg/m^3), high hardness. It is only stable in inert atmospheres at high temperatures.
Aluminum oxynitride (AlON)	Transparent polycrystalline ceramic material with a spinel typed structure.	Excellent thermomechanical and optical transparency properties.
Silicon aluminum oxynitride (SIALON)	Hexagonal crystal structure. Available in several kinds such as α-SiAlON, β-SiAlON ($Si_{6-Z}Al_ZO_ZN_{8-Z}$, $0 \leq Z \leq 4.2$, the Z-value represents the number of O atoms replacing N), O'-SiAlON and X-SiAlON.	Density (3240 kg/m^3), electrical conductivity (~10^{-9} S. m^{-1}), flexural strength (760 MPa), elastic modulus (288 GPa), hardness (1430–1850 kg/mm^2), fracture toughness (6-7.5 MPa m $^{1/2}$), CTE (3×10^{-6} °C^{-1}), thermal conductivity (15–20 W/m K), excellent luminescence properties.
Silicon carbide (SiC)	NA	CTE (~4.5×10^{-6} K^{-1}), melting point (~3003.15 K), breakdown electric field (2 MV/cm) and electron mobility (900 cm^2.V^{-1}.s^{-1}), compressive strength (3900 MPa), elastic modulus (410 GPa), fracture toughness (4.6 MPa m$^{1/2}$), thermal conductivity (120 W/m K), hardness (2800 kg/mm^2), chemical inertness, wide band gap, high permissible operating temperatures, resistance to radiation, low chemical activity, stability of electrical characteristics with temperature changes, Susceptible to thermal dissipation and low self-diffusion coefficient.
Silicon nitride (Si_3N_4)	NA	Fracture toughness (5.7–6.1 MPa m $^{1/2}$), hardness (1450–1580 kg/mm^2), elastic modulus (310 GPa), flexural strength (689–830 MPa), low dielectric constant (can be adjusted in the range of 2–8). CTE (3.3×10^{-6} °C^{-1}), bandgap (~5 eV), thermal conductivity (~30 W/m K), relatively low cost, durability. Susceptible to problems such as surface removal difficulties and damage that correspond to a high machining cost. Brittle fracture behavior.
Zirconia (ZrO_2)	Exist in three thermodynamically stable crystalline phases i.e. monoclinic (M) (stable up to 1443.15 K), tetragonal (T) (stable in the range of 1443.15–2643.15 K) and cubic phase (C) (stable >2643.15 K).	Melting point (3053.15 K), high-temperature resistance, wear resistance and corrosion resistance. A tetragonal phase of zirconia is characterized by a high value of strength and hardness as compared to the other two crystallographic phases. Suffers from low-temperature degradation or aging.
Magnesia partially stabilized zirconia (Mg-PSZ)	NA	Compressive strength (1700 MPa), elastic modulus (205 GPa), fracture toughness (6 MPa m$^{1/2}$), CTE (10×10^{-6} °C^{-1}), thermal conductivity (2.5 W/m K).
Zirconia toughened alumina (ZTA)	It contains around 7–25 wt.% unstabilized ZrO_2 or Y-TZP incorporated into an Al_2O_3 matrix.	High hardness, compressive strength (2500 MPa), elastic modulus (330 GPa), fracture toughness (7.3 MPa m$^{1/2}$), CTE (8×10^{-6} °C^{-1}), thermal conductivity (17 W/m K), good corrosion resistance, high insulation, process flexibility, outstanding chemical and thermal stability, low cost and simple processing procedures.
Alumina-toughened zirconia (ATZ)	Contains about 20 % Al_2O_3 and 80% ZrO_2 or Y-TZP	Outstanding thermal and mechanical properties, biocompatible properties, increased fracture toughness, wear-resistance, and lower hardness. Compressive strength (~2600 MPa), elastic modulus (~250 GPa), fracture toughness (8−12 MPa m$^{1/2}$), CTE (~10×10^{-6} °C^{-1}), thermal conductivity (~6 W/m K).
Titanium dioxide or titania (TiO_2)	TiO_2 is amphoteric, although more acidic than basic and polymorphic. Exist in three polymorphs: anatase, brookite, and rutile. The anatase, rutile has tetragonal coordination and the brookite appearance in the orthorhombic coordination. Among these three phases, the rutile phase is more stable than the rest.	Low toxicity, low cost, availability, Strong oxidizing capabilities, and outstanding chemical stability. The energy gap of the rutile phase is ~3 eV (413~ nm), the brookite is ~3/3 eV (~375 nm), and the anatase is ~3.4 eV (~365 nm), compressive strength (680 MPa), fracture toughness (3.2 MPa m $^{1/2}$), CTE (9×10^{-6} °C^{-1}), thermal conductivity (11.7 W/m K).
Titanium carbide (TiC)	Has a face-centered cubic (fcc) NaCl type structure.	Melting point (3533.15 K), Young's modulus (450 GPa), hardness (HV = 3200), the heat of formation (−148.5 kJ mol^{-1}), thermal conductivity (~21 W/m K), highly chemically resistant material and sufficient electrical conductivity.
Titanium silicocarbide (Ti_3SiC_2)	Hexagonal structure with a space group of $P6_3/mmc$. It has three binding modes: covalent bonding, ionic bonding (Ti and C) and weak bonding, which are similar to the van der Waals force (Ti and Si).	Thermal conductivity at room temperature (37 W/m K) and at 1273.15 K (33 W/m K), Vickers hardness (4 GPa), CTE (9.1×10^{-6} K^{-1}), Young's modulus (322 GPa), temperature coefficient of resistivity (0.00328 K^{-1}), density (4520 kg/m^3), electrical resistivity (0.227 μΩ m), electronic conductivity at ambient temperature (4.4×10^4 S cm^{-1}), high-temperature oxidation and corrosion resistance, easy machinability, better stability.
Titanium diboride (TiB_2)	It has a hexagonal lattice structure (C_{32}) with a space group of P6/mmm.	High elastic modulus, hardness (Vickers hardness = 33.7 GPa and Mohs hardness = >9), high resistance to corrosion and wear, and fair chemical inertness in metal melts and excellent thermal shock resistance, electrical conductivity (9–15×10^5 S/cm). melting temperatures (~3498.15 K), good chemical inertness, and low densities (4520 kg/m^3), good creep resistance, rarely reacting with molten metals and electro-discharge machining capability. Brittleness and oxidation features.

Table 2 (*Continued*)

Ceramic materials	Phases/Bonds/Forms	Properties
Titanium carbonitride (TiCN)	Has a face-centered cubic (fcc) NaCl type structure, belonging to the Fm-3 m space group	Good mechanical properties, high temperature strength, thermal and chemical stability, good corrosion resistance, excellent biocompatibility, and cost-effectiveness.
Silicon dioxide or silica (SiO_2)	Presents two general structural states (crystalline and amorphous). Exists in three main phases (quartz, tridymite, and cristobalite), and five minor phases (coesite, keatite, faujasite, fibrous and melanophlogite).	High chemical stability, low cost, non-toxic, dielectric constant (∼50–100) and has a good impact on environmental compatibility.
Zirconium silicate or zircon ($ZrSiO_4$)	NA	High dielectric constant (∼15), decomposition temperature (>1943.15 K), hardness (7.5 Mohs), linear CTE (∼2.5–4 × 10^{-6} °C^{-1}), fracture toughness (2.1 MPa m $^{1/2}$), thermal conductivity (15 W/m K), high index of refraction (1.96), high corrosion resistance, excellent chemical stability, much cheaper than ZrO_2. $ZrSiO_4$ may decompose into amorphous ZrO_2 and SiO_2 during the oxidation process.
Calcium zirconium silicate or Baghdadite ($Ca_3ZrSi_2O_9$)	Exhibit three kinds of Ca sites in $Ca_3ZrSi_2O_9$ structure (CaO_7 decahedron, CaO_6 octahedron, and CaO_8 quadrangular antiprism).	Excellent cytocompatibility.
Mullite ($Al_6Si_2O_{13}$)	Has a chain structure	Melting point (2103.15 K), flexural strength (180 MPa), compressive strength (1310 MPa), elastic modulus (151 GPa), fracture toughness (2 MPa m $^{1/2}$), thermal conductivity (6 W/m K), CTE (5.4 × 10^{-6} °C^{-1}), good chemical stability, great oxidation and thermal shock resistance, relatively high hardness and density (∼3200 kg/m^3), dielectric constant (5.8 at 1 MHz), chemical inertness and appropriated electrical resistivity. Relatively low mechanical performance.
Boron nitride (BN) and BN composite	BN is an analog of carbon and exists in the form of sp^2 bonded hexagonal (h-BN) and rhombohedral (r-BN) or sp^3 bonded quartzite and cubic BN (c-BN) phases, among which the most common forms are c-BN and h-BN.	Excellent physical properties, remarkable thermal and chemical stabilities (e.g h-BN is stable at temperatures up to 1273.15 K in air, 1673.15 K in vacuum and 3073.15 K in an inert atmosphere), density (2270 kg/m^3), melting point (2873.15 K), band gap (∼6 eV).
Boron carbide (B_4C)	Belongs to an R$\bar{3}$m space group, B_4C structure comprise of 12-atom (B_{12} or $B_{11}C$) icosahedra located at the vertices of a rhombohedral unit cell and a 3-atom linear chain connecting icosahedra along the longest body diagonal.	Density (2520 kg/m^3), melting point (2748.15 K), elastic modulus (460 GPa), thermal conductivity (20–30 W/m K), neutron absorption cross-section (∼4000 × 10^{-28} m^2), Vickers hardness (Hv = 37 GPa), bending strength (∼900 MPa), atomic number density (0.11 $Å^{-3}$), relatively low flexural strength and fracture toughness (∼2.2 MPa $m^{1/2}$), inertness towards most of the chemicals, high hardness to weight ratio, low atomic weight, and self-healing capacity. Poor sinterability due to its high melting point or strong covalent bonding in B_4C (covalent bond content > 90%) and low self-diffusion coefficient.
Sodium zirconium phosphate ($NaZr_2(PO_4)_3$)	It crystallizes in a rhombohedral structure with space group R-3c.	Exhibit very low CTE.
Cordierite or magnesium aluminosilicate ($Mg_2Al_4Si_5O_{18}$)	It has three crystal structures: high temperature hexagonal form (α-cordierite, P6/mmc), low temperature orthorhombic form (β-cordierite, Cccm) and meta-stable form (μ-cordierite).	Good thermal shock resistance, CTE (α = 1–2 × 10^{-6} °C^{-1}), high specific resistivity (ρ>10^{12} Ω.cm), fire resistance, low dielectric constant (ε_r = 5–6), compressive strength (350 MPa), elastic modulus (70 GPa), fracture toughness (∼1.5 MPa $m^{1/2}$). Insufficient mechanical properties, density, and low dielectric constant.
Tungsten acid scandium ($Sc_2W_3O_{12}$)	Consists of corner-sharing WO_4 tetrahedra and ScO_6 octahedra.	Exhibits a linear NTE curve within a wide temperature range of 10.15–1200.15 K without phase transition and NTE behavior may continue to the melting point of 1913.15 K, CTE (−11 × 10^{-6} °C^{-1}).
Tungstate-zirconium (ZrW_2O_8)	ZrW_2O_8 has three phases; the room stable α-phase, a high-temperature stable β-phase, and high-pressure stable γ-phase.	Although ZrW_2O_8 is thermodynamically stable only from 1378.15–1530.15 K, it can be quenched to room temperature and then remains kinetically stable on heating to about 770 °C, and NTE coefficient (about −9 × 10^{-6} K^{-1}).
Silicon oxycarbide (SICO)	Composed of an amorphous SiOC phase, (where Si is tetrahedrally bonded to either carbon or oxygen to form SiO_xC_{4-x} bonds) and a disordered "free carbon" phase.	Offers flexible refractive index which can be tuned in a range from 1.35 to 2.85, high temperature resistance, high creep, resistance against oxidation at harsh environments, tuneable thermal and electrical properties, mechanically strengthened by the presence of tetrahedrally coordinated carbon atoms, not sensitive to air or water.
Silicon boron oxycarbide (SiBCO)	NA	Stable electrical properties and high-temperature resistance.
Hafnium carbide (HfC)	NA	CTE (6.6 × 10^{-6} K^{-1}), hardness (∼26 GPa), melting point (4232.15 K), ideal mechanical properties, strong resistance to oxidation and ablation, high temperature phase stability, and low vapor pressure.
Hafnium nitride (HfN)	Show a rock salt structure with a lattice constant of 4.525 Å.	Negative enthalpy of formation ($\Delta H°_{298}$ = −369.0 kJ mol^{-1}), melting point (3653.15 K), hardness (16.3 GPa), resistivity (33 μΩ·cm), high thermal stability, and chemical inertness.
Hafnium diboride (HfB_2)	Possesses a hexagonal structure.	Melting point (∼3653.15 K), density (11200 kg/m^3), Young's modulus (480 GPa), hardness (28 GPa), high thermal conductivity (104 W/m K), excellent resistance to thermal shock and oxidation, poor sinterability and low fracture toughness.
Zirconium diboride (ZrB_2)	Possesses hexagonal structure.	Lightweight, CTE (5.9 × 10^{-6} °C^{-1}), melting point (∼3518.15-3519.15 K), density (6085 kg/m^3), Young's modulus (450 GPa), hardness of (14–23 GPa), excellent electrical (1 × 10^7 S/m), thermal conductivity (57.9–60 W/m K), fracture toughness (2–3 MPa $m^{1/2}$), low volatilization rate, good chemical stability, and good ablation resistance, inherent brittleness, and weak oxidation resistance, poor sinterability due to strong covalent bonding and leaning to brittle fracture.
Zirconium carbide (ZrC)	NA	Melting point (3693.15–3813.15 K), hardness (25.5 GPa), density (6600 kg/m^3), good thermal and electrical conductivity, excellent phase stability, poor oxidation resistance due to strong covalent bonds and low self-diffusion coefficient, lower cost, low fracture toughness, poor sinterability, and poor thermal shock resistance.

Table 2 (*Continued*)

Ceramic materials	Phases/Bonds/Forms	Properties
β-wollastonite (β-$CaSiO_3$)	NA	Dielectric properties (ε_r: 5, tan α: 1.0–3.0 × 10^{-4}), good thermal stability and high compressive strength and brittle.
Magnesium orthotitanate (Mg_2TiO_4)	Possesses a spinel structure.	Microwave dielectric properties (ε_r: 14.51), quality factor (161570 GHz), τ_f of −49.3 ppm °C^{-1} (1753.15 K), high refractive index and wide-bandgap.
Magnesium titanate ($MgTiO_3$)	Possesses rhombohedral structure with space group R3c.	Bandgap energy (2.82–3.7 eV), relative dielectric constant (∼17), quality factor (160,000 GHz at 7 GHz), resonant frequency (−50 ppm °C^{-1}), and phonon frequency (410–605 cm^{-1}).
La_2NiMnO_6	Crystallize in two distinct crystallographic structures; a higher temperature rhombohedral ($R\bar{3}$) structure and a low temperature monoclinic ($P2_1/n$).	Exhibit both magnetic and electric properties even at room temperature with Curie temperature (∼ 280 K), and activation energy (0.17 eV).
Lanthanum cobaltite ($LaCoO_3$)	Show rhombohedral geometry with symmetry R-3^{-}C.	Good oxidation power, excellent catalytic and electrochemical activity. At ≥373.15 K, $LaCoO_3$ shows paramagnetic property due to transition in spin and at low temperature, it behaves as diamagnetic.
Copper-based complex oxides ($YBa_2Cu_3O_{7-\delta}$)	Exhibits an orthorhombic structure. $YBa_2Cu_3O_{7-\delta}$ consists of tetragonal perovskite cell (P4mm), repeated three times along the c-axis.	Critical temperature (> 90.15 K) and the critical current density are above 77.15 K (> 10^6 A/cm^2).
Lanthanum chromite ($LaCrO_3$)	Exist in three different solid phases (orthorhombic, rhombohedral and cubic) depending on the temperature	Optical band-gap (∼3.4–3.5 eV), melting point (2763.15 K), the electrical conductivity of $\sigma_{800\,°C\ air}$ = 0.96 S/cm, excellent chemical stability in oxidizing and reducing atmospheres.
Tungsten trioxide (WO_3)	n-type semiconductor. Crystallize into several distinct polymorphs, the most common are the monoclinic (m-WO_3) and hexagonal (h-WO_3) phases.	Bandgap (∼2.6–3.1 eV), valence band potential (about +3.49 eV), cheap, non-toxic and earth-abundant, insoluble in water, high stability in acidic solutions, good sensitivity for O_3, NO_x, NH_3 and Cl_2, lower sensitivity to some reducing gases (such as CO, acetone, ethanol), non-toxic, cost-effective, ability to absorb reasonable fraction of solar spectrum.
Beryllium oxide (BeO)	Possesses both covalent and ionic characteristics. Crystallizes in the hexagonal wurtzite structure at ambient conditions, although it can transform into many polymorphs at some conditions such as under in-plane strain or at high-pressure.	Melting point (∼2843.15 K), electrical resistivity (>10^{14} Ω cm), hardness (1250 kg/mm^2), thermal conductivity (∼300 W/m K), transparency over wide spectral range (121–7000 nm), thermal neutron cross-section (10 mb), bandgap (10.6 eV), dielectric constant of (∼6.9), high toxicity in powder form and high sensitivity to light, and resistant to most chemical agents.
Aluminum titanate (Al_2TiO_5)	Exhibit orthorhombic crystal structure with lattice parameters of a = 3.591, b = 9.429, and c = 9.636 Å.	CTE (∼1 × 10^{-6} K^{-1}), high melting temperature (2133.15 K), high thermal shock resistance, good corrosion resistance, and thermal conductivity (0.9–1.5 W/m K), and Young's modulus (10–20 GPa). Al_2TiO_5 is thermodynamic stable only at high temperatures and often requires high temperature reactive firing for microstructural control or reactive sintering to seek densification.
Magnesium dititanate ($MgTi_2O_5$)	Exhibit Rthorhombic pseudobrookite-type structure	Thermal stability (<1873.15 K), low CTE, low thermal conductivity, and high thermal shock resistance, high melting point (∼1950.15 K), low electrical conductivity at ∼1273.15 K (∼2.0 × 10^{-2} S/m), low-cost and non-toxic. Difficulty in obtaining phase purity in $MgTi_2O_5$.
Calcium copper titanate (CCTO)	Exhibit body-centered cubic (bcc) with Im3 space group	Bandgap (∼3.4 eV), electrical sheet resistivity (8.22 Ω/sq), excellent dielectric material, having a very high dielectric constant (ε′ = ∼10^4–10^5), dielectric loss tangent (tanδ) (0.05 at 1 kHz), high dielectric losses and low breakdown voltage.
Barium titanate ($BaTiO_3$)	Displays successive phase transitions showing cubic → tetragonal → orthorhombic → rhombohedral symmetry changes upon cooling.	Good piezoelectric and electro-magnetic properties, high dielectric, ferroelectric, mechanical, thermal, and biocompatibility properties, high dielectric constant (∼10^3) in the range from 100 Hz to 1 MHz.
Strontium titanate ($SrTiO_3$)	n-type semiconductor crystallizes in a cubic structure ($Pm\bar{3}m$) with a room temperature lattice parameter of 3.905 Å, transitioning to a tetragonal structure (I4 mcm) at 105.15 K.	High value of dielectric constant, tunable bandgap (3.2 eV), large electron-hole diffusion length, high thermal stability, high melting point, relatively low ionic and electronic conductivity, strong oxidizing power and long-term stability, conduction band edge (∼0.2 eV), non-toxicity, and low dielectric loss.
Lead zirconate titanate or PZT or $Pb(Zr_xTi_{1-x})O_3$	PZT perovskite may take up a tetragonal, rhombohedral or orthorhombic structure at room temperature	Excellent dielectric and piezoelectric properties, optical absorptance and high power-handling capability.
Lithium niobate ($LiNbO_3$)	$LiNbO_3$ crystals belong to the triangular system with space group symmetry R3c, which is characterized by the ilmenite-type structure	Large spontaneous polarization, along with unique nonlinear optical properties, large pyroelectric coefficient, small dielectric constant, low acoustic losses, brittleness, high ferroelectric transition temperature (1483.15 K), strong spontaneous polarization at room temperature (70–80 μC/cm^2).
Lead titanate ($PbTiO_3$)	Exists in two crystal structures; cubic phase (Pm-3 m) of a = b = c =3.887 Å and tetragonal phase (P4 mm) of a = b = 3.9022, c = 4.1437 Å.	Good dielectric, ferroelectric and pyroelectric properties, band gap (3.4 eV), high phase transition temperature (763.15 K), low dielectric constant at room temperature (∼200).
Lead zirconate ($PbZrO_3$)	PZO can exhibit an antiferroelectric phase or paraelectric phase depending on the temperature. At temperatures below 493.15 K, $PbZrO_3$ has an orthorhombic perovskite structure with an antiferroelectric character. At temperatures above its curies temperature T_c (503.15 K), PZO changes to the cubic perovskite structure with a paraelectric character.	High energy density, and high permittivity.
Bismuth ferrite or bismuth ferric oxide ($BiFeO_3$)	Exists as rhombohedral distorted perovskite structure.	High open-circuit voltage (50 V), energy bandgap (2.0–2.7 eV), curie temperature (∼1103.15 K) and antiferromagnetic Néel temperature (∼643.15 K), non-toxic, poor quantum efficiency and slow carrier mobility.
Lithium tantalite ($LiTaO_3$)	Crystallizes in polar noncentrosymmetric space group R3c.	High mechanical and chemical stabilities, low acoustic losses, brittleness, melting temperature (1923.15 K), high coercive field (∼21 kV/mm) for polarization reversal.
Zinc titanates ($ZnTiO_3$)	Exists as cubic-$ZnTiO_3$ and hexagonal-$ZnTiO_3$.	Electron mobility (0.015–0.4 m^2/Vs), optical band gap (∼3.6 eV), low sintering temperature and good dielectric properties, high reduction potential and low oxidation potential. Susceptible to rapid recombination of photogenerated electrons and holes.

Table 2 (*Continued*)

Ceramic materials	Phases/Bonds/Forms	Properties
Zinc oxide (ZnO)	NA	Electron mobility (0.2–0.3 m^2/Vsec), optical band gap (~3.37 eV), high exciton binding energy (60 meV), low toxicity, low cost, excellent stability, and environmental friendliness. Susceptible to rapid recombination of the photo-created e^-/h^+ pairs and high defect density.
Tin dioxide (SnO_2)	Exists as point group $D^{14}{}_{4h}$ with space group p42/mnm	Bandgap at room temperature (~3.6 eV), high chemical and thermal stability, high theoretical capacity (790 mA h g^{-1}), high optical permeability, relatively low conductivity, high exciton binding energy (130 meV), cost-effective and non-toxic.
Hydroxyapatite ($Ca_{10}(PO_4)_6(OH)_2$)	NA	Excellent bioactivity, osteoconductivity, biocompatibility, biocompatibility, and good mechanical properties, non-toxic, environmentally benign, and low cost.
Molybdenum disulphide (MoS_2)	MoS_2 has three different crystal structures including 1T-MoS_2 (tetragonal symmetry), 2H–MoS_2 (hexagonal symmetry) and 3R–MoS_2 (rhombohedral symmetry).	Resistant to dilute acids and water, high theoretical capacity (670 mA h g^{-1}), Bandgap (1.3 – 1.8 eV), high mobility of charge carriers and excellent optical absorption properties. Suffers from serious fast capacity fading caused by low conductivity owing to intrinsic semiconductor characteristics, and leads to poor reaction kinetics and rate capability, and easy agglomeration.
Cadmium sulfide (CdS)	n-type semiconductor	Direct bandgap (2.4 eV), low quantum efficiency and photocorrosion, a high rate of recombination of electron-hole pairs, high electron mobility and excellent transmission characteristics. Superior light absorption, good carrier transportation capacity, suitable flat-band potential, and easy agglomeration.
Uranium dioxide (UO_2)	NA	Low thermal conductivity. Can withstand high temperature (~2573.15 K), density (10,970 kg/m^3).
Gallium nitride (GaN)	GaN can crystallize in the hexagonal structure or wurtzite	bandgap (~3.4 eV), breakdown electric field (~3.3 MV/cm), and high saturation-drift velocity (~3×10^7 cm/s), thermal conductivity (0.47 W/m K), melting point (2600.15 K), can operate at higher voltage and temperature, threshold energy for radiation hardness (440 KeV), high electron mobility at room temperature (~0.1 $m^2 V^{-1} s^{-1}$),
Cuprous sulfide or chalcocite (Cu_2S)	p-type semiconductor material. Exists in three different forms at various synthetic temperatures, namely, low-chalcocite γ-phase with monoclinic (M) symmetry (below 369.15 K), high-chalcocite β-phase with hexagonal (H) symmetry (between 369.15–699.15 K), and digenite α-phase with cubic structure (above 699.15 K).	Bandgap (1.2–1.8 eV), high theoretical capacity, good electron conductivity (10^{-3} S cm^{-1}) and high-temperature range (699.15–999.15 K).
Nickel oxide (NiO)	p-type semiconductor	Low cost, low temperature processing, and higher activity, wide-band-gap (~3.4−4 eV), high hole mobility, wide bandgap, non-toxicity, reproducibility, great sensitivity, and chemical stability, poor electron conductivity, severe volume changes during discharge/charge processes, ultrahigh theoretical capacitance (2584 F g^{-1}), excellent electrochemical reactivity, and environmental friendliness. Suffers from slow ion diffusion rate, poor electrical conductivity, and weak cycling stability.
Manganese monoxide (MnO)	NA	Theoretical capacity (756 mA h g^{-1}), eco-friendly, intrinsically poor electronic conductivity (10^{-8}–10^{-6} S. cm^{-1}), serious aggregation in addition to manifest volumetric change throughout lithiation and delithiation reactions, high density (5430 kg/m^3), low cost, environmentally friendly, high abundance of Mn, melting point (1923.15 K).
Indium tin oxide (ITO) (Sn-doped In_2O_3)	n-type semiconductor.	Low resistivity (~7×10^{-5} Ω cm), high visible light transmittance (≥90%), high infrared reflectance, good chemical stability, abrasion resistance, and electrical properties, high cost due to the limited reserve of indium, bandgap (~4.7 eV).
Mica ($KAl_2(Si_3Al)O_{10}(OH)_2$)	NA	High melting point (1149.15–1299.15 K), good thermal stability at high temperatures even up to 1273.15 K, temperature tolerance extends up to 873.15 K.
Lithium-zirconium oxides or lithium metazirconate (Li_2ZrO_3)	NA	Low activation, good neutron multiplication characteristics of Zr, compatibility with structural materials, reprocessing.
Copper oxide (CuO)	p-type semiconductor	Narrow band-gap energy (~1.2–1.6 eV), non-toxic, abundant, and inexpensive, and shows unique physical and chemical properties.
Magnesium aluminate spinel ($MgAl_2O_4$)	NA	High melting point (2408.15 K), low dielectric constant (8.75 at 12.3 GHz), high quantity factor (68,900 GHz at 12.3 GHz), and relatively low temperature coefficient of resonant frequency (−75 ppm/°C), CTE (~7.6×10^{-6} K^{-1}), high mechanical strength both at room temperature (135–216 MPa) and elevated temperatures (120–205 MPa at 1573.15 K) and excellent resistance to slag corrosion.
Strontium barium titanate ($Sr_{1-x}Ba_xTiO_3$, BST)	NA	Chemically, physically and electrically more stable.
Cobalt monoxide (CoO)	Exist as rocksalt structure (fcc).	High theoretical capacitance (5722 F.g^{-1}), the bandgap of 2.2–2.8 eV, high theoretical specific capacity (715 mA h g^{-1}), high earth abundance, low cost and nontoxicity. Low electrical conductivity and huge volume stress in the cyclic process.
Calcium titanate ($CaTiO_3$	It has distorted orthorhombic structure below 1380.15 K with space group Pbnm	High recombination rate of photoexcited e^-/h^+ pairs, wide bandgap (~3.4 eV), elative dielectric constant (160), temperature coefficient of the resonant frequency (850 ppm/°C), and quality factor (3600 GHz at 7 GHz).
Magnesium oxide (MgO)	Exist as cubic crystal structure with Fm-3 m space group	High surface area, and unusual crystal morphology, low cost, wider optical energy gap (7.3 eV), non-toxic, high specific surface reactivity, large bandgap (≈3.5 eV).

Table 2 (*Continued*)

Ceramic materials	Phases/Bonds/Forms	Properties
Magnesium aluminum oxynitride (MgAlON)	NA	Possess low linear CTE ($5.3 \times 10^{-6}\,K^{-1}$ - $7.4 \times 10^{-6}\,K^{-1}$) and a high thermal conductivity at room temperature (10.89 W/m K) which means better thermal shock resistance and excellent spalling resistance.
Vanadium pentoxide (V_2O_5)	n-type semiconductor. Exists as polymorphic phases that include α-V_2O_5, β-V_2O_5, γ-V_2O_5, and δ-V_2O_5	Possess indirect bandgap (2.0 eV), direct bandgap (2.4 eV), low melting temperature (~963.15 K), cost-effective, has several oxidation states, theoretical capacity (~1472 mA h g^{-1}).
Lanthanum hexaboride (LaB_6)	Exist as a simple cubic structure with the Pm3 m space group.	Free carrier density ($1.45 \times 10^{22}\,cm^{-3}$), low work function (~2.4–2.6 eV), high melting point (2988.15 K), and good stability under ion bombardment, low evaporation rate, low fracture toughness (1.8 MPa $m^{1/2}$).
Cobalt (III) oxide (Co_2O_3)	NA	Melting point (1168.15 K) and density (5180 kg/m^3).
Diamond	NA	High strength and extreme hardness, weak bonding strength to a substrate, large bandgap (5.5 eV), elite thermal conductivity (>2000 W/m K), high breakdown field (>10 MV/cm) and high carrier mobility (> 0.2 m^2/Vs).
Yttrium oxide or yttria (Y_2O_3)	NA	Excellent chemical inertness, high corrosion resistance, transparency range (0.8–2.0 μm), bandgap (5.8 eV), and refractive index (>1.9).
Lead lanthanum zirconate titanate (PLZT) $Pb_{1-x}La_x(Zr_yTi_z)_{1-x/4}O_3$	Possesses a perovskite-type (ABO_3) structure	Piezoelectric coefficients (d_{33} = 710 pC/N, k_p = 0.72), low loss, high optical transparency, a broad range of composition and outstanding electro-optic properties.

NTE: Negative thermal expansion; CTE: coefficient thermal expansion; Q × f: quality factor.

freeze casting and phase inversion. Table 3 shows the disadvantages and advantages of each fabrication process. In the following sections, the aforementioned methods will be described in detail.

Dry forming

There are two main methods involved in dry forming including uniaxial die pressing (UDP) and cold isostatic pressing (CIP). One main advantage in the dry forming process is that it does not require drying, and as such eliminates the problems of drying shrinkage (like cracking risk during drying, drying time as well as saves energy on the cost of drying). As compared to uniaxial die pressing, CIP shows superiority in terms of complexity in its shape, whereas in terms of precision, it is inferior as compared to powder injection molding (PIM). UDP is a low-tech and simple fabrication method for simple prototyping, mass fabrication of simple shapes, production of blanks for subsequent green machining (example in making orthopedic hip bearings). It is one of the most widely forming processes of ceramic components. The process is usually conducted at low-to-moderate pressures as more pressure results in problems (like non-uniformity of sintered components and delamination). Basically, UDP involves dry ceramic powders (usually fed into a uniaxial hollow die), with the addition of a little amount of organic binders and liquid.

CIP is used where there is a requirement of complex-shaped or extremely large ceramic components, where injection molding is not practical, beyond the shape-capabilities of UDP, and the requirement of a large production volume. CIP has particle packing uniformity and superior shape capability in comparison to UDP. It involves the placement of a dry-ceramic powder in a thin-walled soft "mold," or "bag" that is generally made of an elastomer like polyurethane silicone, latex, nitrile or neoprene. In most cases, the mold or bag is shaped. In other cases, a ceramic powder pre-form is inserted in a sealed elastomer bag. The bagged preform or powder is immersed in an oil chamber and is subsequently pressurized. Typically, the pressures in CIP can be ~70 MPa, although pressures >100 MPa to ~400 MPa are often used. The depressurization and pressurization cycles should be conducted at a slow controlled rate so as to prevent the damage of the green component from sudden application reduction or stress reduction.

Wet forming methods

Wet forming method also has the main benefit of shape complexity, with large negative effects in terms of the need for drying (in the case where H_2O is the liquid medium) or binder removal (gel casting and injection molding) because of three associated problems such as the cracking risk during drying, drying time and the energy costs for drying. One key disadvantage is the drying shrinkage, with ceramic powder compact having little cohesion, and so cracking becomes the real risk. During drying, some of the key issues that require addressing include the particle size, PSD, solids loading, drying times and component size. For instance, the finer the size of the particle, the greater the shrinkage which will result in a higher risk of cracking. Also, finer particles tend to enhance the sintering process. As the PSD becomes broader, shrinkage becomes lower which will result in a lower risk of cracking. As the solids loading becomes higher (minimized liquid), the shrinkage tends to be lower, which will lower the cracking risk. Less liquid will cause the ceramic green body to be less workable as well as less suitable to precision mold filling which as a consequence will require a very high forming pressure. Longer drying time will assist in the reduction of cracking, As the components become larger, the cracking risk and total shrinkage becomes larger. Some high-tech solutions used for drying such as controlled humidity chambers, supercritical CO_2 drying, and ethylene glycol. All these factors add complexity, cost, and time to the production process.

Powder injection molding

The powder injection molding (PIM) or ceramic injection molding has long been considered the premier process of production for high precision ceramic components. The PIM process involves first the preparation of the feedstock by the mixture of ceramic powder with up to ~40 wt% thermoplastic polymer binders, organics or waxes. After hot mixing and then cooling, the feedstock is granulated into pellets and then subsequently fed into the molding machine. Basically, the mold and molding machine should be designed to accommodate the problem of erosion from the abrasive ceramic-binder mix. The granulated feedstock is then heated to about 523.15 K to produce a flowable paste before its being injected into the mold, under high pressure. After component removal and cooling from the mold, the next process is to debinding which is a critical process due to cracking risk. Firstly, most of the binder is removed or dissolved by chemical or/and thermal approach. Thereafter, the final residue is removed as a burn-out stage in the process of sintering. For smaller components, mold tooling may be designed to accommodate multi-components. There are two key issues of great significance associated with PIM in ceramics including wall thickness and draft angle. Uniformity and minimization of wall thickness are essential for distortion reduction during the removal of binder. However, a

Table 3
Advantages and disadvantages of ceramic components fabrication methods.

Fabrication methods	Advantages	Disadvantages
Wet pressing (in comparison with dry pressing)	It can produce complex geometries.	There is a need for drying.
	Density distribution is uniform.	Compaction is lower. Tolerance is higher.
Uniaxial die pressing (UDP)	Drying is not necessary.	Simple-shape capability.
	Ease of automation.	Non-uniformity of particle packing which can result in cracking during sintering, distortion and non-uniform firing shrinkage.
	Maximum production and rate Better tolerance control.	High upfront capital cost. Die degradation via abrasion.
Cold isostatic pressing (CIP)	In comparison to UDP:	Limited dimensional control.
	Possibility of more complex-shapes. It can greatly reduce pressing pressure gradients (cracking and distortion).	Superiority in shape complexity to UDP. Inferior in shape complexity to PIM.
	In comparison to other forming methods:	Powders for CIP require excellent flowability (need for spraying drying or mold vibration during filling).
	Cost of mold is low. No mold cost for post-CIP. No size limitation. High density with no textures. No density gradients. Short processing cycle times.	Low cycle times.
Powder injection molding (PIM)	Production is fast.	Risk of cracking.
	Cost of labour is low. Flexibility in design. High production output. The use of multiple materials at the same time. Possibility of producing very small parts. Post-production of scrap is minimal. Inserts can be included. Good dimensional-control and colour-control. Good product consistency. The requirement for finishing is reduced.	Energy and time consuming. High tooling and machines cost. Binder removal is problematic. Restricts part design. Small runs of parts can be costly.
Tape casting	High degree of automation with simple equipment. low production cost with high production efficiency. Capable to achieve flexible homogeneous ceramic body as well as large size products with less downstream processing. Continuous production. Thin layers. Good dimensional accuracy	Drying is necessary. Limited part geometries.
Slipcasting	Wide variety of complex geometries can be produced (thin walls, asymmetric). Low capital investment and material consumptions. Highly homogeneous slurries can be produced.	Rough surfaces. Wall thickness can be difficult. Difficulty to prepare ceramic slurry (the exact ratio of water and ceramic powder is important). Complex rheology. Difficulty in the manufacture of mold. Lower dimensional precision (high dimensional tolerance). Lower production rate. Problem of differential shrinkage.
Extrusion	Production is continuous. High production capacity. High part lengths. Environmental and economically friendly (only powders and water are used).	Distinct textures. Drying is necessary. Variations in size. Limited complexity of the parts.
		Costly and time consuming due to repetitive sintering steps.
Green machining	Eliminates all risks and problems involved in processes capable of shape complexity. Eliminates drying problems. Closer dimensional accuracy. Additionally, requires finishing operations to obtain desired characteristics.	Requires more energy, capital and labour for material removal. Longer operation time.
Additive manufacturing (3D printing)	Little-skill manufacturing.	High production costs and slow build rates.
	Less waste. No assembly required. Complexity.	Post-processing is required. Production process can be discontinuous. Component size is limited. Mechanical properties are poor. Serious consideration should be given to application design and setting process parameters.
Gel casting	Pressure injection at high temperature is not required. Binder removal stage is less problematic.	Toxicity problem of the polymer component. Automation is not easy.

Table 3 (*Continued*)

Fabrication methods	Advantages	Disadvantages
	Elevated strength as well as the processability of the green body. Great density. Little cost. Low shrinkage during sintering and drying. Casting and solidifying processes are controllability.	Insufficient strength after gelation for handling post-casting. Susceptible to high cracking during drying.
Thixotropic casting	Water based. No binder. Processing is simple.	Low densification rate during sintering. Difficult in demolding.
Freeze casting	Simple, flexible and inexpensive process Complex shapes can be cast that require zero machining Casted products have an excellent surface finish and accurate dimensional tolerance and are lightweight, Near-net shapes can be achieved. It is capable of fabricating highly porous engineered parts with small processing shrinkage. High mechanical strength is reasonable Non-tortuous continuously graded columnar pores	Lack of control of nucleation conditions. Difficulty in controlling more complex lamellae orientations.
Direct foaming	No additional template is needed. No fugitive pore formers have to be burned out.	Narrow range of pore characteristics. Difficult removal of binders Costly and intricate Shrinkage and drying stresses. Difficulty in controlling the metastable wet foam state
Phase inversion	It requires fewer procedural steps and it is less complicated. Capable of producing flat, tubular, spiral wound or hollow fiber configuration. High surface per volume ratio. Mechanical properties are high. Production volume is high. Capable of obtaining the desired structure by varying important parameters.	The rate of the demixing process must be controlled. Difficulty in solvent selection. Environmental effects of used organic solvents.

thinner wall might also be problematic with distortion risk during debinding (because of its fragility). In order to enable the ease of removing mold, the draft angle is generally required to protrude features of the molded component. For instance, a square protrusion with totally parallel walls is likely to break when removed from the mold. Meanwhile, if the walls are slightly-tapered by 1 or 2°, this will assist during the release of mold. If the components are ejected from the mold before they are fully cool and shrunk around the mold, removing the mold may become easier and the draft requirement is avoided.

Tape casting

Tape casting was first introduced by Glen N. Howatt in the mid-1940s for the production of thin piezoelectric materials [9] and has proven to be a versatile approach for fabricating manufacturing thick film and thin film insulator components. In 1947, Howatt [10] published his first paper on the fabrication of thin ceramic sheets for capacitors. In their study, the slurry was prepared by a mixture of ethocel V-495 resin, albalyn, staybelite, toluol, type 50, TiO_2 and diethyl oxalate and subsequently tape cast via a 325-mesh screen. Tape-casting involves the production of thin-sheet ceramics from a ceramic powder slurry, generally, a non-aqueous slurry containing various plasticizers, additives, and binders to produce a dried tape which is quite robust for post-processing [11]. The tape-casting is a process of feeding the slurry through a micro screed referred to as the doctor blade, which screeds the slurry into a thin layer of fixed thickness, and then is rapidly dried via evaporation (Fig. 1). This is similar to the concrete screeding but on a sub-millimeter thickness scale. The thickness of a single green tape can be controlled by adjusting the gap between the blade and component. Also, green tapes can be tailored and laminated to the desired thickness (determined by adjusting the doctor blade width) and shapes.

Some specific organics have also been used as binders, dispersants, and plasticizers in the process of tape casting while cracking or deformation usually occurs during organics debinding as well as removing or sintering process. In order to obtain a ceramic components with relatively large sizes without deformation, many influential factors must be considered during preparation including powder characteristics (PSD, particle size, specific surface area), the solids loading, suspending solvent type used to form the slurry, concentration and composition of additives (deflocculants, binders, plasticizers), doctor blade gap, relative velocity, and drying parameters (hold time, drying temperature, and heating rate).

According to the solvent nature of the slurries, tape casting is divided into two categories such as non-aqueous and aqueous tape casting [12]. The drawbacks of aqueous media include slow drying rate, low tape green strength, heightened crack sensitivity, increased agglomeration due to hydrogen bonding, and possible material reactivity with H_2O. These limits their practical applications significantly, even though the approach contributes to the reduced impact on health and environment hazards, a more manageable process and lower cost. Non-aqueous tape casting has a wider range of options for additives, uniform green structure, low surface tension, low boiling point, shortened production time and high tape green strength. Therefore, it is extensively used in industrial production. Non-aqueous tape casting like organic tape casting is based on larger toxicity of organic solvent like xylene, toluene, benzene, etc., which are toxic, cost-intensive, and environmentally harmful. Furthermore, the comprehensive performance of the relative dielectric constant and the surface tension of mixed solvent are better than that of a single solvent [13], and effectively increase the solubility of the binder and thus avoids cracking in the drying process of ceramic tape.

The tape casting process is considered comparable to traditional slip casting in the ceramic industries as the fluid suspension of ceramic powders/particles is also used as the starting point for processing.

Slip casting

Slip casting is specifically for making hollow components/shapes (although it can be used for curved and flat tiles [15]), which

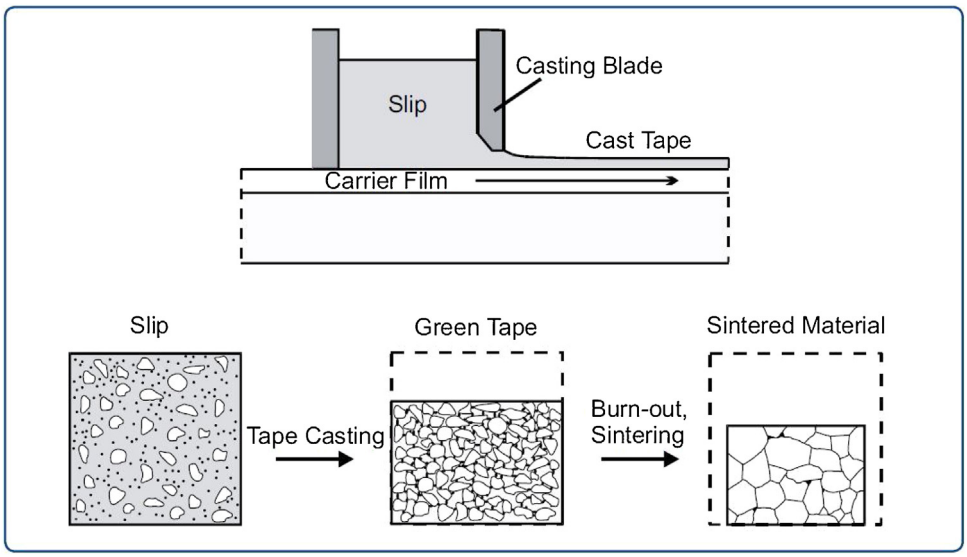

Fig. 1. The top schematic drawing illustrates tape casting. The bottom sketch shows the different stages during the processing: the slip consisting of H_2O, ceramic particles and binder; the cast, dried green sheet; and, finally, the microstructure of the sintered material [14].

is low cost and combines shape simplicity with complexity as compared to other component processing techniques. Slip-casting involves the process of filling a porous mold, usually a mold, with a ceramic slurry (Fig. 2). Slip casting is one of the most commonly used industrial methods for ceramic processing which provides accurate control of the microstructure in cast porous materials and high dispersion degree of ceramic phases [16,17]. Additionally, the colloidal processing implies the formation of suspensions in aqueous media, which is a draw-back in the case of both metal particles and non-oxide ceramic, due to the elevated reactivity of these materials with the suspension media [18]. Four major components are required of a slip-casting slurry such as the ceramic powder (ball-milled to sub-micron size range), demineralized water (to aid the careful control of suspensions conditions) [19], chemical deflocculant (helps to optimize the contents of solids and in maintaining colloidal stability of slurry) and organic binder (to impart green strength). In slip casting, the possible molds range that can be cheaply and easily fabricated is almost limitless. The molds usually have low toughness and high porosity, which lowers the strength. If the strength is to be increased, some porosity must be sacrificed. Low-strength gypsum molds tend to wear out with time because the pores eroding from H_2O passing through them. These molds are usually great for the production of complex shapes because as the green body loses H_2O and starts drying out, it shrinks away from the edges of the mold for ease of removal. This is good because the time to remove damaged components is reduced.

Extrusion

Extrusion is another forming method where the ceramic slurry is extruded via a die and produces articles of semi-infinite length with fixed cross-section. Extrusion is carried out by the die at its exhaust instead of using the injection mold. This process was first invented in 1619 by John Etherington for the production of brick. It is commonly used for the manufacturing of bricks, pipes, as well as ceramic tubing. It involves the preparation of a plastic mix of ceramic in a solvent (mostly H_2O) with deflocculant, binder, and other additives like plasticizers [15]. The process of ceramic extrusion involves five steps as shown below [20]: (a) blending (b) pugging (c) extrusion (c) cutting and drying (e) sintering

During blending, the moisture content of the slurry is controlled by mixing ceramic powders with a suitable surfactant, binder, coagulant, lubricant, deflocculant, preservatives, and plasticizer. For lubricant selection, there are various lubricants commonly used such as silicones, stearates, colloidal talc, and petroleum oil. Due to the high flow stress and the poor ductility of ceramics, the extrusion process is preferable to conducted under a slower speed and higher temperature to avoid fracture as well as reduce flow stress.

Other ceramic forming methods

The number of ceramics forming methods is large. Ceramic components have also been fabricated via gel-casting, thixotropic casting, direct foaming, freeze casting, and phase inversion.

Gel casting

Gel casting is a promising forming process developed to overcome some of the limitations of other complex shape techniques like slip casting and injection molding [1]. Since its development in Canada in the 1960s, it has evolved into an attractive ceramic forming process to manufacture large-sized, near-net-shape, complex ceramic parts, high-quality with defined threshold strength [34]. This process does not shrink the powder compact in the mold or remove any component. Rather, dispersing the medium is either solidified via polymerization or via trapping voids or molecules within the particle system. The process starts with the preparation of a slurry by using a monomer as a solvent. Thereafter, the slurry is cast in a mold and is then polymerized [15], which is followed by debinding and sintering. Gel casting also shares some common or specific features and key differences with PIM: (1) the binder content in gel casting is about 5–10 times less than binder used for PIM, thereby allow the binder removal process to be less-problematic. (2) gel casting entails a simple pouring of ceramic slurry into a non-porous mold and involves no requirement for pressure injection at high temperature and all associated tooling and machinery of PIM.

There are two main considerations to be put in place when producing ceramic components using gel casting. First, it is important to determine the optimal gelation speed which must be fast enough to ensure the foam does not collapse. Second, the gel rheology must enable all details of the mold to be filled and as such, gels of high fluidity are required, especially for producing highly complex shapes [22]. The steps in this process include pre-mixing,

casting, drying, and sintering. Gel casting should not be confused with sol-gel processing. In gel casting, the precursor (ceramic powders) is suspended in a monomer/polymer solution to produce slurries for casting. The monomer or polymer solution gels without reacting with the suspended powder, locking the particles in place; the same gel would be formed in the absence of any ceramics. In sol-gel processing, ceramic precursors are integral to the gel formation process (through polycondensation, hydrolysis, etc.) hydroxides, metal alkoxides produce the backbone of the gel network and are converted to ceramic in later processing steps [23].

Thixotropic casting

Like gel casting, thixotropic casting has shown great promise but has failed in becoming the mainstream in the industrial process of ceramic component manufacturing due to the extreme solids loading applied as well as the no or little drying shrinkage. Thixotropic casting is a vibratory casting of highly thixotropic slurries/paste having high solids loadings such that they become fluid only under vibration [15]. The techniques explore the high packing ability of ceramic powders that have trimodal and/or bimodal size distribution to produce such concentrated suspensions. However, the different densification rates of the coarse-sized and fine-sized particles and the use of relatively coarse particles can hinder the complete component densification during sintering. In thixotropic casting, extremely high contents of solids are achieved by blending fine, medium and coarse powder grades in optimized ratios in addition to chemical deflocculant (extreme thixotropy can be achieved using a powerful chemical deflocculants).

Direct foaming

Direct foaming method has been developed and is a process where an alkane phase is emulsified in an aqueous ceramic powder suspension [24]. In direct foaming, a ceramic suspension is foamed by gas incorporation (chemical or physical blowing); the wet foam is stabilized, dried and sintered. In this process, an extremely high porosity of ~97 % can be obtained. It is a low-cost operation and its flexibility is high when adjusting the final microstructure and chemical composition. The key aspects are the consolidation and stabilization mechanisms. Wet foams are thermodynamically unstable systems in which processes such as gas bubble coarsening and drainage of the liquid-phase lead to final destruction and foam degradation. The drainage corresponds to the flow of the liquid phase due to the gravitational effect. Reducing the liquid-phase content will amount to a closer approach to the bubbles leading to their coalescence [24]. Gas diffusion occurs between bubbles of different sizes and consequently different gas concentrations due to the difference in Laplace pressure between them [17]. These mechanisms of foam degradation are driven by the reduction of the Gibbs free energy of the system. Therefore, it is of fundamental importance to activate further stabilization effects to control the natural evolution of the foamed powder suspensions as well as to provide adjustment of the cellular ceramic microstructure [24].

Wet foams and emulsions are used in a wide range of technological applications, especially in food technologies and cosmetics. In addition, emulsions can be used as templates to determine the porosity parameters in inorganic porous structures. In the case of surfactant stabilized emulsions, the structure is normally set via sol-gel processes, which requires controlled chemical reactions, cannot be easily applied to different compositions and consumes time [25,26]. The use of particles for the long term stabilization of emulsions can be applied to produce a porous ceramics of different compositions without the necessity of chemical reactions for the consolidation of emulsions [27]. Ceramic foams that are obtained by direct foaming are attractive because they are easy to be processed, providing reliable pore sizes from μm to mm scale in combination with an accessible open cell microstructure [28].

Freeze casting

Freeze casting is a solidification route capable to produce functionalized ceramic components with highly-tunable porosity and has attracted a lot of consideration due to its versatility, environmentally friendly character, and simplicity. Furthermore, water can be used both as a pore former or template and as a solvent [29]. Freeze casting involves physical interactions rather than chemical interactions, and the freeze cast microstructure is not strongly dependent on the materials' chemical composition. During solidification of a solution or suspension, walls are templated due to the particle's rejection or/and solute by a solidifying fluid. The shape, size, volume fraction, and orientation of porosity templated during the process may be tuned via a change in the suspension characteristics (such as particle fraction, additives, fluid type) and solidification conditions (such as freezing components material, mold design, freezing component temperature, and solidification technique). However, this freedom also adds significant complexity during an attempt to understand the underlying principles which govern the microstructure templated during freeze casting [30].

In summary, freeze-casting starts with preparing the stable aqueous or nonaqueous colloidal suspension, pouring the suspension into the mold, molded suspension freezing, sublimating the solidified phase under reduced pressure, and sintering to consolidate a porous structure [31]. Fig. 3 shows a schematic illustration of the steps involved in the freeze casting of ceramic components. In

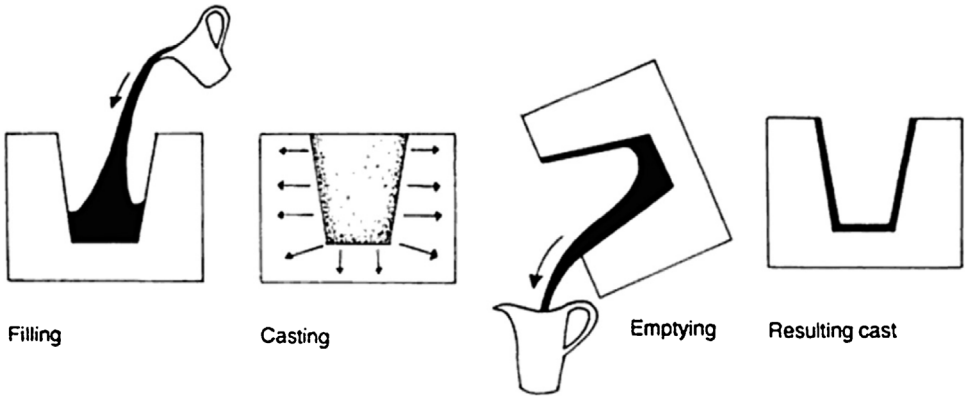

Fig. 2. Steps involved in slip casting [20,21].

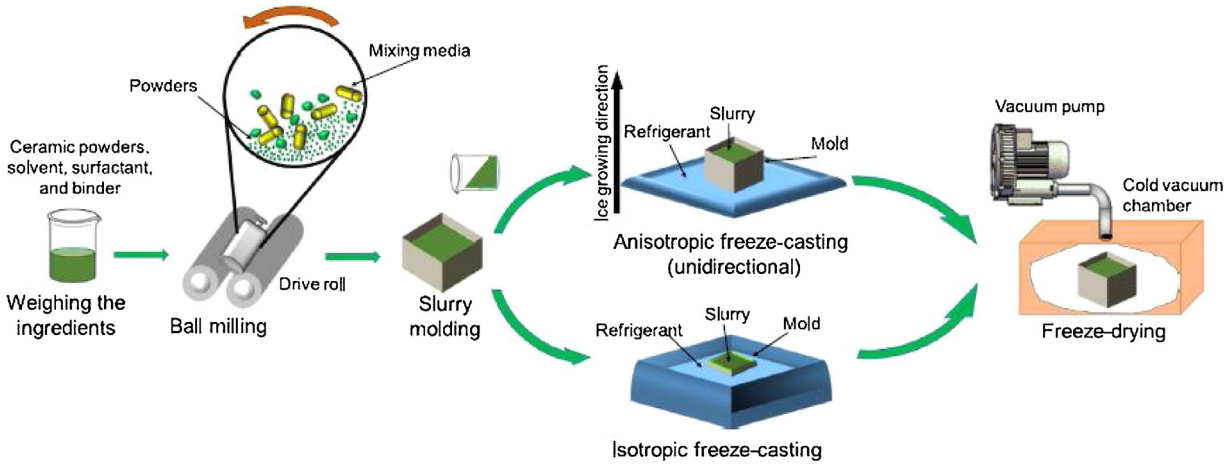

Fig. 3. Schematic representation of the freeze-casting process for ceramics components [32].

freeze casting, solvent nucleation proceeds after placing a suspension onto a freezing substrate. The propagation of frozen dendrites in the thermal gradient direction pushes the particles away, and the frozen solvent is then removed via sublimation [32]. Particles redistribution must occur to form a porous freeze cast structure. The particles that are suspended in the slurry are propagated by the growing solvent crystals and are accumulated between the ice crystals arms [33]. In other words, the particles in the slurry have to be rejected from the solidification front and collected between the adjacent frozen channels. Fig. 4 shows the segregation of particles in the slurry, propagated by the growing crystals of solvent and particle accumulation between the frozen channels. The generated ice crystals are then removed by vacuum sublimation, thus creating a highly permeable porous structure that can be sintered at the desired temperature. Depending on the state and composition of the colloidal suspension as well as the freezing rate, numerous porosities types can be achieved with this route [34]. The presence of highly permeable channels of the green bodies and absence of sacrificial pore formers like temporary binders allows the use of high heating rates which consequently shorten considerably the thermal treatment cycles.

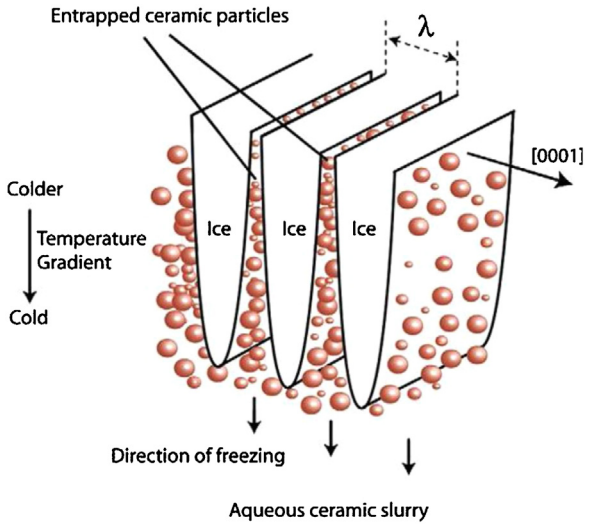

Fig. 4. Ice crystals formation and particle segregation during freeze casting of ceramic slurries (λ is the wavelength of the structure) [32,35].

Freeze casting solidification techniques can broadly be categorized as isotropic and anisotropic. Anisotropic, usually referred to as unidirectional solidification is more extensively investigated than isotropic techniques as solidification typically takes place in a vertical manner (i.e. bottom to top). In this process, a particle suspension or a solution containing dissolved ceramic material is poured into a mold. Typically, the base and top of the mold are composed of thermally conductive base like copper and a thermally insulating side like Teflon. The base of the mold is cooled, thereby promoting nucleation and directional propagation of a solidification front. At first, the solidification velocity is very high and suspended particles or/and solute are initially engulfed by the solidification front. This results in a dense particle layer at the sample base [30,36]. The latent heat released by such early freezing events slows the velocity of solidification and particles are subsequently pushed by the solidification front rather than engulfed, forming a solute/particle accumulation region ahead of the front [37]. As solidification progresses, rejected particles or/and solute are concentrated within interdendritic space, where solidification of interstitial fluid occurs eventually. Once solidification is complete, the solidified fluid is removed through sublimation, and the resulting scaffold is sintered to densify particle packed-walls. After sublimation and sintering, the resulting pore structures are nearly isotropic [38]. However, depending on the isotropic technique employed, pore structures range from closed, equiaxed cells (when space-holder techniques and isotropic freezing are combined) [39] to open, reticular [40] networks. In some cases, thermally conductive molds are used and freezing progresses directionally from the bottom as well as radially from the sides [41]. Although, some microstructural directionality is often observed in the resulting material (especially at the bottom and radially), causing the structure to be nearly isotropic. Isotropic freeze casting techniques are commonly used for freeze gelation; in such cases, the solution precursor or suspension undergoes a cross-linking or gelling stage prior to the freezing process [42].

Phase inversion

Phase inversion involves a demixing process whereby the initially thermo-dynamically stable solution is transformed in a controlled manner from a liquid to a solid-state [43]. At a certain stage during demixing, the most concentrated liquid-phase will solidify to form a solid matrix. Such transformation can be achieved in several ways such as controlled evaporation of solvent from three-component systems, immersion precipitation via

immersion in a nonsolvent, precipitation from the vapor phase and via the thermally induced phase separation [44,45]. One main difficulty which limits the successful casting in phase inversion is the lack of a systematic and predictable method in the selection of solvent systems [46]. Among the mentioned techniques, immersion precipitation and the thermally induced phase inversion are the commonly used technique for the fabrication of ceramic components.

The early development of phase inversion ceramic membrane was reported by Luyten et al. [47] for the preparation of $LaSrCoFeO_{3-x}$ hollow fiber membranes (HFM) for the production of cost-effective oxygen. The membrane was obtained using a mixture of ceramic powders as a major component while reducing the polymer content. The polymer acted as a binder in the mixture and is burned-off during the sintering process. As a typical suspension preparation method, ceramic powders with solvent are milled for 24 h, followed by further mixing for more than 24 h after polymer addition. Then, the suspension is extruded using a double cylinder nozzle which is placed close to the non-solvent bath.

Applying the phase inversion method, regions of different pore sizes are formed in the components without the need for a multi-step process which is onerous due to constraint of the sintering process at high-temperature in each step [48,49]. This approach is the main technique to produce ceramic membranes.

Sintering of ceramics

Sintering process occurs through the bonding of particles upon heating via bulk mass transfer and surface-transport mechanisms, with its main goal being to obtain a fully dense solid component (some residual porosity remains in most cases). The bonds that are formed between the pre-existing bonding within the particles and the sintering particles are identical. The driving force being heat together with the elimination of surface energy. Basically, as the specific surface area of the powder becomes higher, the sintering also becomes better. Sintering correlates with many factors such as sintering temperature and time, green density, agglomerates, pressure, heating and cooling rate, sintering atmosphere (vacuum or nitrogen, air, argon, hydrogen, water vapor), grain size, porosity, particle size, shrinkage, and liquid-phase sintering. Among the aforementioned factors, the most important parameter is temperature because it presents an exponential effect. The surface energy per volume is inversely proportional to the diameter of the particle. For instance, particles with smaller diameter have more surface energy and can sinter more rapidly. A higher density of ceramics is preferable as it reduces shrinkage during firing. Higher density of ceramics can be achieved by higher loading of solids, higher pressing pressures, deliberately graded fine/medium/coarse particle blends or broader PSD. For example, sintering efficiency can be reduced if coarsest particle size is much. A soft agglomerate is broken down during the forming process whereas, a hard agglomerate will compromise sintering thereby causing residual pores.

If volatilization occurs like binder burn-out, the heating rate should be slower. For instance, large ceramic cross-sections require a heating rate that is slower to accommodate thermal diffusion and also prevent harmful thermo-mechanical stresses, which will evolve from thermal gradients. Moreover, slower heating rates can influence the degree of sintering in the presence of short soaking times. As the cooling rate becomes faster, the thermal shock risk is higher due to thermo-mechanical stresses developed from thermal gradients. With an increase in sintering time and temperature, grain growth increases. Generally, grain growth is undesirable due to a reduction in the mechanical properties of the ceramic components. Grain boundaries are defective regions with high atomic mobility and play a crucial role in the late sintering stage. The goal of sintering is to eliminate or minimize porosity except in the case involving a porous ceramic component like a tissue scaffold or nano-porous filter. Firing shrinkage is increased by lower green density and higher specific surface area/finer particle size. The incorporation of flux agents such as alkali earth ions as well as silicates will create a glassy phase that helps to enhance sintering and then concentrates on the grain boundaries. For lower purity ceramics (like low-end wear tiles, armor panels, and spark plug insulators), liquid phase sintering is desirable whereas it is undesirable for ultrapure or high-performance ceramics [15].

According to temperature difference, sintering can also be classified as ultra-low temperature co-fired ceramics (ULTCC) (sintering temperature <973.15 K), low temperature co-fired ceramics (LTCC) (sintering temperature 973.15–1223.15 K) and high temperature co-fired ceramics (HTCC) (sintering temperature >1223.15 K). ULTCC technology enables cost reduction and better miniaturization compared to LTCC technology. HTCC and LTCC technologies are extensively used in the fabrication of hybrids in microelectronic devices. LTCC is a well-known technology, which has been used for the fabrication of multilayer components. Advantages such as a high versatility in the fabrication process and excellent dielectric properties have deemed LTCC as a typical solution for radio frequency and microwave devices. One important disadvantage of LTCC is high surface roughness, which complicates its application as a components for the growth of active circuit elements including transistors, which structure preferentially utilize single crystalline materials [50,51]. It has similarities with the more conventional multilayer printed circuit board in its configuration, but this ceramic technology is highly suited for microwave and radio frequencies as well as for hash operating environments where high mechanical stresses and high temperatures are prevalent. LTCC materials generally have the following characteristics such as suitable CTE for matching with other materials in integrations, high thermal conductivity, low dielectric loss, low relative permittivity for fast signal transmission [52]. The characteristics of HTCC technologies are high temperature stability, excellent mechanical stability, easy integration into metal housings due to matched thermal coefficients of expansion via good thermal conductivity and high temperature brazing. HTCC substrate-based components have vast application channels in microelectronic integrated packaging technology, 3D multichip modules applications in military, aerospace engineering, gearbox control in automotive applications, medical, and engineering management systems [53].

Sintering can also be classified into two major categories according to pressure difference namely the pressureless and pressure sintering. The former involves heating of the formed compact to about two-thirds of its melting temperature at ambient pressure and holding time while the latter employs the simultaneous use of temperature and pressure (densification during sintering). In solid-state sintering/pressureless sintering, densification occurs by solid-state, diffusion-controlled mass transport. Since mass transport occurs faster through a liquid than through a solid, densification occurs faster in the presence of a liquid phase. Liquid-phase sintering requires a liquid phase (melt) that is chemically compatible, that wets the particles, and that dissolves some of the solid. In a system containing multiple phases, such as cermets, the sintering temperature must be between the melting point of the phase that forms the melt and that of the other phase (s). many non-oxide powders with covalent bonds between the constituting elements are difficult to sinter by solid-state sintering because mass transport by diffusion is low, even at high temperatures. In some cases, sintering additives are added that form a liquid phase. For example, the addition of a few percent of certain oxides to Si_3N_4 leads to liquid silicate phases during sintering. In comparison to pressureless sintering, pressure sintering is more

expensive, does not allow to produce complicated shapes, and is not suited for mass production. On the other hand, pressure sintering lowers the sintering temperature or allows faster sintering at the same temperature than pressureless sintering. Pressure sintering is usually used in manufacturing ceramic components that are difficult to sinter without pressure such as non-oxide ceramics. The most common technique is called hot pressing. A powder is compacted in a die and pressed uniaxially between two forming rams while heated to high temperatures. Hot isostatic pressing is like the cold isostatic pressing used in ceramic components fabrication, except that the pressing is done at the sintering temperature. The pressuring medium is typically a gas, in most cases argon.

Besides these methods, several non-conventional techniques have been applied to fabricate ceramic component sintering such as microwave sintering, dynamic or shock consolidation as well as field assisted sintering. Microwave sintering is characterized by reduction in processing times and temperature gradients due to coupling of direct energy with electric dipoles within the heating body [54]. The reduction in processing time gives the final property benefits by reduction in grain growth which can be achieved by by-passing the low-temperature region where the grain growth rate is higher than the densification rate. Dynamic or shock consolidation occurs due to the passage of large amplitude compressive stress generated by plate explosion/impact, whereby no external heating is applied. Thus, densification proceeds by plastic resulting to high temperatures due to particle inter-friction which enables good interparticle bonding. One major drawback of dynamic or shock consolidation is the difficulty in coordination of the heat generation events and short stress waves, which frequently leave components fractured.

Spark plasma sintering (SPS) allows a very rapid heating rate and cooling rate, a short holding times and preparation of fully dense components at comparatively low sintering temperatures, which is lower than the normal hot sintering. Instead of using an external heat source, an electrical current (AC or pulsed DC, DC,) is passed through the conducting pressure die and/or through the sample. In this way, the die acts as the heat source and the sample is heated from both outside and inside. Factors that contributes to the process of rapid densification includes the exposure to an electric field, fast heating rate and cooling rate, as well as a mechanical pressure, which exceeds the normally used hot pressing processes. The SPS method has found applications in laminated structures of dissimilar ceramics such as $CoFe_2O_4$, TiN/Al_2O_3, TiB_2/SiC, $(TiN)_x(Al_2O_3)_{1-x}$ [54–58], metastable constituents like α-sialons, and to prepare a dense-compacts containing nanosized grains like Al_2O_3. Other field assisted sintering methods are pulse electro discharge consolidation or field activated sintering technique, plasma activated sintering which have effectively been applied to nano-powder consolidation [59].

Finishing of ceramic components

Ceramic component in its processed state has some individual properties due to minor changes which are uncontrollable during the process. Because of gravitational effects and differential shrinkage during the sintering process, these can accumulate to minimum of 1%–2% distortion. This is in contrasts with similar polymeric or metallic components, where in-processing dimensional stability within a fraction of 1 % is maintained. Thus, to bring these advanced ceramic components to a common standard, machining is usually a requirement. Machining or green machining is a controlled surface destruction of ceramic components to produce desired strength, size, shape, and finish. It generally involves a blank manufacturing via UDP, proceeded by precision computer numerical control (CNC) machining, and then sintering. Furthermore, it combines shape complexity with the elimination of all associated cracking risks and problems of drying in PIM and CIP [15]. Machining of sintered ceramics are often done when it is impossible in achieving the necessary dimensional tolerance with other techniques like optimization of ceramic component forming and sintering to avoid deformation, densification shrinkage minimization (for example, via reaction bonding of Si_3N_4, SiC, Al_2O_3), and white (after a pre-sintering) or green (before sintering) machining. One major drawback is the high machining cost of sintered ceramics. Some other finishing processes also exist to finish fully sintered advanced ceramics including lapping, grinding, turning and polishing, milling or drilling.

Grinding involves the abrasive grits bonded onto a wheel, rotating at high speed. The orientation of the individual grains is random; thus, a grain may encounter the working surface with a negative, zero, or positive rake angle. Grinding varies in geometry such as surface grinding with vertical or horizontal spindle, internal grinding, cylindrical grinding, centerless grinding as well as plunge (form) grinding [60]. Honing technology is applied to mechanically finish brittle-hard ceramics, thereby rendering the smoothest surface texture with greatest accuracy. There are many variants of honing like round, screw, plane, plunge and profile honing (long-stroke) as well as super-finishing (short-stroke). The long-stroke allows for a high surface quality and provides the possibility of a smooth finish of internal cylindrical surfaces to have a form accuracy and high dimensionality. The short-stroke (super-finishing) honing finds its applications in sliding surfaces and machining friction, parts of anti-friction bearings and slide bearing pivots, as well as seats and sliders of packing collars and rings [61].

Polishing and lapping are techniques with loosed abrasives and function by sliding frictions between a surface and particles. The polisher or lap travels across a work surface against which particles of mud-type slurry or sand is forced to the point of contact. The work piece tends to show a planetary movement and acquires a flat, uniformly-machined and is randomly-finished. Due to high cost for machining of advanced ceramics components, several near net shape technologies have been introduced for complex-shaped components production with the need for machining at minimal. Near net shape processes involve the control and optimization of each step of the process of production, thus minimizing the size and number of microstructural defects to within design limits [62]. A typical example is the injection molding which is suitable for the production of near-net shape of ceramic components which requires little subsequent grinding, while eliminating the requirement for machining. PIM allows a wide range of component shapes and sizes for various ceramic materials to be produced [63]. Other suitable methods to produce near-net shape components includes the colloidal forming methods like direct coagulation casting, gel casting, clay-like forming as well as hydrolysis-assisted solidification.

For decades, several innovative near-net shape techniques were developed including temperature-induced forming (TIF) or solid freeform fabrication (SFF). The SFF technique allows the manufacture of a mold-free ceramic components by addition of materials via layer by layer. Current SFF techniques are selective laser sintering, laminated object manufacturing, stereolithograph, fused deposition of ceramics and 3D-printing (selective laser sintering, inkjet 3D printing, and electron beam melting). In TIF method, the consolidation of a highly-filled slurry is achieved by facile temperature increase. As it does not involve the removal of dispersing media, nonporous molds can be used for shaping [59].

Recently, 3D printing has revolutionized many industries and is also making a significant impact in the ceramic component industry. Till date, the principal application of 3D printing in the ceramic industry is in prototyping and research but is increasingly applied for short-production runs and is also ideal to manufacture

specialty components. Specialist biomedical applications of ceramics particularly lend themselves to 3D printing given the high value adding feature and shape complexity requirement.

Applications of ceramic components

According to their functions, advanced ceramic materials can be classified into two categories (electro-ceramic materials and the advanced structural ceramic materials). In advanced ceramics, the pure and high-quality powders (as presented in Table 2) form the basis. These powders, with sub-micron grains and narrow grain size distribution obtained from a synthetic production route are processed in various steps into green body with special properties (high physical and mechanical properties). They are hard and strong due to their strong covalent and ionic bonds between the elements. Table 4 presents the classification of advanced ceramics materials under various functions and applications.

In the past decades, research efforts have been focused on the development of ceramic components exhibiting a wide domain of applications due to their unique electrical, thermal, mechanical, magnetic, chemical, superconducting, optoelectronic, properties. These applications include biomedical applications, energy transformation, supply and storage, transportation systems, information technology, pervaporation, antifogging, anti-frosting and anti-corrosive applications, wastewater and water treatment, and manufacture technology. Table 5 also present the summary of some advanced ceramic components used in various applications. In the following section, we also described their various applications.

Electronics

The use of ceramic component has proven to be very attractive in multitude of electronic applications (such as automotive, telecommunication, power electronics, integrated circuits, filters, circulators, oscillators, thermally stable resonators, isolators, phase shifters, di-electric resonator antennas in microwave, millimetre wave communication and various radar and sensor systems) as they can operate at high temperatures, high frequencies and power, harsh environments, and also combine properties including magnetism and electrical insulation, which are impossible for polymers or metals. Good thermal stability, low-loss tangent, and low dielectric constant are primary requirements for ceramic materials to achieve efficient signal transmission. Low-loss ceramic materials used in the circuit improves its overall quality factor by reducing the insertion loss and the power dissipation, which suppresses the electrical noise in oscillators and can produce non reciprocal devices, low-loss phase shifters and highly selective filters [135,136]. Furthermore, by selecting a low-loss

Table 4
Specific ceramic materials under various functions and applications.

Categories	Function	Applications	Specific ceramic materials
Electro-ceramics	Electrical	Conductors	B_4C, $LaCrO_3$, TiC, TiN
		Super conductors	$YBa_2Cu_3O_{7-\delta}$, $PrBa_2Cu_3O_{7-\delta}$, $YBa_2Cu_2O_7$
		Semi-conductors (thermistors, varistors)	ZnO, SnO_2, GaN, SnO_2, CdS, CoO, MoS_2, WO_3, BN, V_2O_5, ITO, $MgTi_2O_5$, Cu_2S, AlON, $ZnTiO_3$, $CaTiO_3$, CuO, CdS, SiC, $SrTiO_3$, Cu_2S, GaN, NiO, MnO, CoO, $BaTiO_3$, $BiFeO_3$, NiO, $LiNbO_3$, BeO, ZnO, TiO_2, TiC, HfN, ZrW_2O_8
		Insulators	$MgAl_2O_4$, Al_2O_3, MgO, $SrTiO_3$, SiO_2, SIALON, BeO
		Ferroelectric random memory	(Ba, Sr) TiO_3, PZT
		Non-linear conductors	SiC, CuO, PTC/NTC, V_2O_5, $LiNbO_3$, $LiTaO_3$
	Electronics	Electron emission	BaO, $SrTiO_3$, ZrW_2O_8, LaB_6
		Piezoelectric	$LiTaO_3$, $MgTiO_3$, ZnO, $LiNbO_3$, $LiTaO_3$, $BaTiO_3$, PZT, AlN, $LiCoO_3$,
		Magnetic	Ferrites, NiO, Co_2O_3
	Mechanical	Heat resistant	Si_3N_4, SIALON, SiC, $Mg_2Al_4Si_5O_{18}$
		Lubrication	BN, MoS_2
		Machinable	Mica ceramics, BN composite
		High strength	TiC, SiC, Si_3N_4, TiN, Diamond
		Water-resistant	B_4C, SiC
		Porous	SiO_2, Cordierite
	Optical	High refraction	ZrO_2, TiO_2, $MgAl_2O_4$, B_4C, BeO, TiC, Al_2TiO_5, SiC, mullite, Diamond, $Mg_2Al_4Si_5O_{18}$, $ZrSiO_4$
		Translucent	Al_2O_3, SIALON
		Photoconductive	CdS, GaN, Cu_2S
		Photocatalysts	TiO_2, ZnO, NiO, CuO, CoO, $LiNbO_3$, CdS, MoS_2, $BiFeO_3$, $PbTiO_3$, Al_2O_3, Cu_2S, $SrTiO_3$, WO_3, $CaTiO_3$, ferrites, $ZnTiO_3$, CCTO, $ZnTiO_3$, $MgTi_2O_5$
		Transparency	Y_2O_3, ITO, SnO_2, ZnO
		Photochromic	WO_3
		Kerr Effect	Lead lanthanum zirconate titanate
		Phosphorescent/ fluorescent	Nd_2O_3, Er_2O_3
	Thermal	Low thermal expansion	SiO_2, Cordierite, Al_2TiO_5
		High thermal expansion	Al_2O_3, AlN, SiC, BeO, MgO, Si_3N_4
		Heat insulation	Si_3N_4, ZrO_2
Structural	Bio/chemical	Chemically resistant	SiC, Al_2O_3, TiB_2, BN
		Bioactive	HAP, $BaTiO_3$, $Ca_3ZrSi_2O_9$
		Bio inert	Al_2O_3, ATZ, ZrO_2
		Membranes	SiC, $LaCrO_3$, SiO_2, Al_2O_3, TiO_2, ZnO, SiOC, mullite
		Catalyst	$LaCrO_3$, CuO, CoO, $MgAl_2O_4$, NiO, MnO, $ZnTiO_3$, SnO_2, $BaTiO_3$, Cu_2S, $MgTi_2O_5$
	Atomic energy	–	UO_2, SiC, B_4C, BeO, HfB_2, ZrB_2, ZrC, Ti_3SiC_2
	Cutting tools	–	Diamond, ZrC, HfB_2, Si_3N_4, TiB_2, ZTA, B_4C, ZrB_2, TiCN, Ti_3SiC_2, TiC, SIALON
	Aerospace	–	Al_2O_3, SiC, Si_3N_4, ITO, AlN, ZrB_2, HfB_2, TiCN, ZrO_2, TiC, Si_3N_4
	Tribological	Wear resistant	SiC, ZrC, HfN, B_4C, ZTA, TiCN, Ti_3SiC_2, TiC, ZrO_2
	Automotive	Sensors, Heat engines	Y_2O_3, CuO, LaB_6, MgAlON, V_2O_5, NiO, $ZnTiO_3$, SnO_2, $SrTiO_3$, MoS_2, ZnO, ZrB_2, $LaCrO_3$, GaN, Ti_3SiC_2, $ZnTiO_3$, Si_3N_4, B_4C, SiC, HfB_2, PZT, CCTO, Al_2TiO_5, $Sc_2W_3O_{12}$, $Mg_2Al_4Si_5O_{18}$, SiOC, SIALON, Al_2O_3
	Bone	–	ATZ

Table 5
Summary of some advanced ceramic components used in various applications.

Ceramic	Fabrication method	Shape of components	Information on component preparation	Sintering parameters	Components modification	Properties of component/remarks	Application	Ref.
ZrO_2	Cold isostatic pressing	Cylinder	NA	NA	Brazing with Mo-particle-reinforced Ag-Cu-Ti	A maximum shear strength of 370 MPa was realized.	Biomedical	[64]
ZrO_2	Non-aqueous tape casting	Round tape	Firstly, C_2H_5OH and $C_4H_8O_2$ (volume ratio 50:50) were mixed to prepare the non-aqueous solvent. ZrO_2 powder was subsequently introduced into the mixture, and then their mixture was ball milled for 1 day; DBP and PVB were added. Finally, the obtained slurry was ball milled for 24 h and later degassed for the 30 s.	Temp.: 1753.15 K; Time: 1 h	NA	Thickness: 200–280 μm;200–280 μm; Relative density: 98%; dielectric: 32. The prepared ceramics show defect-free surfaces, good quality, uniform pore distribution, low porosity, and proper light transmission.	NA	[65]
α-Al_2O_3	Direct foaming	Circular Spawning tiles	HAPES was prepared using decane and stabilized α-Al_2O_3, as alkane based organic solvent and ceramic material, respectively. An emulsified suspension was prepared by adding 0.33 vol.% SLS and 70 vol.% decane to the previously stabilized aqueous Al_2O_3 suspension under continuous stirring.	Temp.: 1673.15 K; Time: 2 h	Oxygen plasma sputtering	NA	Aquaculture	[66]
Al_2O_3	Direct foaming	Spawning plates	An aqueous Al_2O_3 suspension was prepared, thereafter decane was added to the slurry via emulsification and using HAPES. This is followed by stirring, transferring the stabilized emulsified suspension to the flat mold, followed by drying.	Temp.: 1673.15 K; Time: 2 h	Wet chemical silanization using hexadecyltrimethoxysilane followed by subsequent O_2 plasma treatment	Convenient geometries.	Aquaculture	[28]
α-Al_2O_3	Direct foaming	Foams	Dry Al_2O_3 was slowly added to DI H_2O containing 0.74 wt.% which relates to Al_2O_3 under severe mixing. Thereafter, an emulsified suspension was prepared by adding 0.33 vol.% anionic surfactant and 70 vol.% decane to the ceramic suspensions.	Temp.: 1823.15 K; Time: 2 h; HR: 2 K/min; CR: 3 K/min	Blending with HAPES	Porosities: ~90 %; cell sizes: 3–200 μm.	NA	[26]
α-Al_2O_3	Direct foaming	Round foams	The suspension was prepared using DI H_2O and α-Al_2O_3. PAA was added to stabilize the suspensions.	Temp.: 1823.15 K; Time: 2 h	Blending with HAPES	Porosities: ~97.5 %; cell sizes: 0.5–3 mm.	NA	[24]
(0.01) Oriented Al_2O_3	Slip-casting	Target	4.0 N purity ZnO–(2 wt% nominal) Al_2O_3 powders using DI H_2O (no deflocculant).	Temp.: 1873.15 K	DC-sputtering deposition of ZnO: Al	Roughness value: 0.21 nm.	NA	[67]
$Mg_{0.95}Ca_{0.05}TiO_3$	Extrusion	wafers	2 wt% of HDPE was added into the dried ceramic powders.	Temp.: 1653.15 K; Time: 4 h	NA	Favorable microwave properties with εr:~20; tan δ: < 10^{-4}.	microwave antenna	[68]
Al_2O_3	Phase inversion	Flat sheet membrane	NA	NA	Two-step hydrothermal method of TiO_2 NRAs	NA	Photocatalytic	[69]
Al_2O_3	NA	Thin films	NA	Temp.: 1273.15 K	Screen printing of $Ca_{1-x}BaxBi_2Nb_2O_9$	NA	Microwave dielectric	[70]
γ- Al_2O_3	Phase inversion	Flat sheet membrane	NA	NA	Electroless plating and annealing	Thickness: <5 mm.	Gas separation	[71]
Al_2O_3	Phase inversion	Tubular membrane	NA	NA	Layer deposition of TiO_2	ID: 7 mm, an OD:10 mm, Length: 100 mm.	Water treatment	[72]
Al_2O_3	Uniaxial die-pressing	Discs	Ulexite extracted from the natural mineral, was added as a binder. Ba,Co or La,Co were thereafter incorporated for catalytical purpose.	Temp.: 923.15 K	Deposit of Ti	NA	Wastewater	[73]

STL/(BNT-BLZT)	Tape casting	Disc	Involves the synthesis of BNT-BLZT and STL powders. TiO_2, $SrCO_3$, and Li_2CO_3 were used as powders to prepare STL. To prepared the STL powders, 0.5 wt% Li_2CO_3 was added into $SrTiO_3$ powders and milled in alcohol for 12 h (to lower the sintering temperature of $SrTiO_3$). Bi_2O_3, Na_2CO_3, TiO_2, $BaCO_3$, La_2O_3, and zirconia were used as initial powders for BNT-BLZT. Glycerol trioleate, butanone and alcohol were milled for 4 h (to obtain the slurries). Then DBP, PVB and PEG and BNT-BLZT or STL powders were added and the mixture was milled for another 4 h.	Temp.: 1448.15 K; Time: 4 h	Lamination	NA	Energy storage	[74]
Al_2O_3	Phase inversion	Circular membrane	Al_2O_3 powder was added into SiO_2 solution (0.6 wt% Na_2O and 30 wt% SiO_2) to produce a solution with Al_2O_3/ SiO_2 of 1:10 in weight. 1H,1H,2H,2H-Perfluorodecyltriethoxysilane was diluted in ethanol to obtain a 2 wt.% FAS solution. The Al_2O_3/SiO_2 and the ethanol/FAS solutions were mixed and stirred vigorously for 24 h.	NA	Coating with 32-μm thick oxide NPs modified fluorinated monolayer	Thickness: 2.4 mm; Diameter: 47 mm; Average pore size: 2.4 μm; Porosity: 42.8 %.	Vacuum membrane distillation	[75]
Ba_2BiSbO_6	Uniaxial die-pressing	Cylinder	$BaCO_3$, Bi_2O_3, and Sb_2O_3 were mixed and milled with ZrO_2 balls for 1 day using C_2H_5OH, followed by drying of slurries. Powders were calcined for 6 h at 1323.15 K, and then ball milled for another 1 day, dried and added with 8 wt % PVA. Thereafter, the powders were pressed into cylinders	Temp.: 1223.15–1423.15 K; Time: 6 h	NA	Optimum microwave dielectric properties (Ɛr) : 26.61; τ_f:-26.6 ppm/ °C.	microwave dielectric	[76]
α-Al_2O_3	Uniaxial die-pressing	Tubular membrane	Al_2O_3 powders were put in nylon jars. DI H_2O and balls of corundum were added at pH 6, milled for a day. The mixture was heated under continuous stirring. After oven-dried at 383.15 K for 48 h and then grinding, the uniform Al_2O_3 powders were passed through an 80-mesh screen.	Temp.: 1673.15–1873.15 K; Time: 2 h; HR: 3 °C/min	Deposition of polydopamine using $CuSO_4$/ H_2O_2 as a trigger and subsequently grafting of hexadecane thiol	Diameter: 30 mm; Thickness: 3 mm.	Wastewater	[77]
Al_2O_3/ 3Y-TZP	Uniaxial die-pressing	rectangular bars and pellets	Al_2O_3/Y-TZP powders were put into the nylon jars. DI H_2O and corundum balls were added into the mixture at pH 6, milled for 24 h. The mixture was heated under continuous stirring. After oven-dried at 383.15 K for 48 h and then grinding, the Al_2O_3/Y-TZP powder mixture was passed through an 80-mesh screen. Simultaneously, PVA (0.15 wt%) and paraffin (3 wt%) were added. The ceramic body of rectangular bars and pellets were prepared at 8 MPa	Temp.: 1673.15-1873.15 K; Time: 2 h; HR: 3 °C/min	NA	Fracture toughness: 3 MPa m $^{1/2}$; Bending strength: ∼90 MPa	NA	[78]
α-SiC	Cold isostatic pressing	Rectangular sheet	NA	NA	Oxidation treatment	NA	NA	[79]
Ti_3SiC_2	NA	NA	NA	NA	Brazing with Ag-Cu-2Ti	NA	NA	[80]
Calcium phosphate HAP	Uniaxial die-pressing	Plane cylindrical	NA	Temp.: 1473.15 K; Time: 2 h; HR: 50 °C/h; CR: 100 °C/h	Micropatterning, CNC-micromachining and laser treatment	NA	NA	[81]
Natural quartz	Radial isostatic pressing	Tubular membrane	Natural quartz (200–400 μm) was used as the main component of the ceramic mixture. H_2O solution of sodium aluminosilicate, flower, clay mineral, non-ionic surfactant (1 wt.% OS-20 solution: a mixture of PEG esters of higher fatty alcohols) were used.	Temp.: 1123.15 K	Coating with mesoporous silicate hybrid organic	NA	Heavy metal ions retention	[82]
γ- Al_2O_3		Pellets				NA		[83]

Table 5 (*Continued*)

Ceramic	Fabrication method	Shape of components	Information on component preparation	Sintering parameters	Components modification	Properties of component/remarks	Application	Ref.
	Uniaxial die-pressing		Ceramic material was uniaxially die-pressed using a hydraulic press to form 1 mm to 2 mm thick pellets of 20 mm in diameter.	Temp.: 1273.15 K; Time: 2 h	Hydrothermal growth of ZnO microrods		Catalytic application	
Calcined diatomite	Uniaxial die-pressing	Pellets	Ceramic material was uniaxially die-pressed using a hydraulic press to form 1 mm–2 mm thick pellets of 20 mm in diameter.	Temp.: 1273.15 K; Time: 2 h	Hydrothermal growth of ZnO microrods	NA	Catalytic application	[83]
Cordierite	Uniaxial die-pressing	Pellets	Ceramic material was uniaxially die-pressed using a hydraulic press to form 1 mm – 2 mm thick pellets of 20 mm in diameter.	Temp.: 1273.15 K; Time: 2 h	Hydrothermal growth of ZnO microrods	NA	Catalytic application	[83]
α- Al_2O_3	Non-aqueous tape-casting	Wafers	First, 1.5 ml of menhaden fish oil was added into the solvents (80 ml abs. C_2H_5OH and 40 ml xylenes). Secondly, the solvents were ball milled for 30 min. Third, 0.05 wt% MgO was added and ball milled for another 30 min. Thereafter, 100 g Al_2O_3 was introduced into the solvents and ball milled for 10 h. 2.5 wt% BBP and 3.5 wt% PEG400 were added into the initial slurry and mixed for 60 min, after which 6 wt.% PVB was added and ball milled for 12 h. Finally, viscous slurry with homogeneous compositions was obtained.	Temp.: 1073.15 K; Time: 10 h; HR: 10 °C/min	NA	NA	NA	[84]
AlN	Uniaxial die-pressing	Disk pellet	First, the KOH and (silicic acid with boric acid) were ball milled 2 h at 400 rpm using distilled H_2O, after being dried, grounded, and calcined at 673.15 K, low melting $0.1K_2O$-B_2O_3-$2SiO_2$ and B_2O_3-$2SiO_2$ powders were formed, respectively. Thereafter, these powders were ball milled together with different content of AlN powder (30 wt%–60 wt%) for another 2 h at 400 rpm using T-butanol. After freeze-drying, $0.1K_2O$-B_2O_3-$2SiO_2$/ AlN composite and B_2O_3-$2SiO_2$/AlN composite powders were prepared, respectively.	Temp.: 1123.15 K; Time: 1 h; HR: 5 °C/ min	NA	When the content of AlN was 40 wt.%, sintered components at 850 °C have thermal conductivity: 1.632 W/(m.K), dielectric constant: 4.93; dielectric loss: 0.0064: flexural strength: 60.26 MPa.	Electronics	[85]
Magnéli phase Ti_4O_7	Isostatic pressing	Preform sheet	Firstly, magnéli phase Ti_4O_7 nanopowders was synthesized by the reduction of TiO_2 nanopowders under an H_2 atmosphere at 1223.15 K. The preformed Ti_4O_7 nanopowders were subsequently mixed with 0.5% (m/m) of a binder consisting of polyacrylamide/ PVA (95/5, m/m) and a certain amount of H_2O to form a slurry, and the slurry was spray-dried to small ceramic granulates (40–80 mesh, 5% moisture content). The ceramic granulates were loaded into a mold, vibrated, and then pressed at 60 MPa for 5 min to prepare the preform.	Temp.: 1623.15 K; Time: 11 h	NA	Magnéli phase Ti_4O_7 ceramic materials in various shapes having extensive interconnecting macropores with average pore size: 2.6 μm; Porosity: 21.6%. Porous Ti_4O_7 ceramic anode exhibited greater PFOA/PFOS oxidation rates than other electrodes.	Electronics	[86]
α- Al_2O_3	Slip casting	Rectangular plate	the α-Al_2O_3 powder was doped with 2 mol% of various metal oxide dopants. Samaria and neodymium and 5 wt.% antimony doped tin oxide were commercially available powders. CeO_2, Mn_3O_4, Fe_2O_3, Cr_2O_3, and NiO were synthesized from acetate or nitrate salts by combustion of these precursors in the air for 3 h at 873.15 K. Al_2O_3 and dopants were dispersed in H_2O using 1 wt% dispersant and 0.5 wt.% binder, the 75 % of solid content. The	Temp.: 1073.15 K, 1773.15 K; Time: 3 h; HR: 2, 5 K/min	Laser-induced selective activation and Autocatalytic metallization	NA	3D interconnect device	[87]

			dispersions were attrition milled with ZrO_2 milling balls for 2 h. Rectangular plates were cast on a pre-dried plaster plate, dried overnight and debindered/pre-sintered at 1073.15 K for 1 h.					
AlN and 3Y- TZP	Cold isostatic pressing	Rectangular Bars	Firstly, 3Y- TZP powder was mixed with 1.5 wt %, PAA-NH_4 (40% in H_2O) to obtain a stable 3Y-TZP suspension. An appropriate amount of Al $(NO_3)_3{\cdot}9H_2O$ (44.5 wt%) and 3Y- TZP suspension were then mixed in a 50 °C H_2O-bath, in addition to using 1 mol/L HNO_3 and 5 mol/L $NH_3{\cdot}H_2O$ as the titration to form $ZrO_2@Al_2O_3$ precursor solution. Afterward, SCS and VFD with $CO(NH_2)_2$ were used to prepare the $ZrO_2@Al_2O_3$ nanopowders. Then, the $ZrO_2@Al_2O_3$ components were pressed into bars at 170 MPa.	Temp.: 1873.15 K; Time: 3 h	NA	When PAA-NH_4 content was 1.5 wt.%, the $ZrO_2@Al_2O_3$ powders with high crystallinity and uniform grain size was obtained. After high temperature sintering at 1600 °C for 3 h, the diffusion of the 3Y- TZP core and the movement were effectively suppressed due to the pinning effect of the Al_2O_3 shell-layer.	NA	[88]
$CoFe_2O_4$	NA	Plate	NA	Temp.: 1223.15 K	chemical solution deposition of Lead zirconate titanate films	NA	Electronics	[55]
Si_3N_4	Uniaxial die-pressing	NA	The mixture (Si_3N_4, MgO and Y_2O_3) was added in a PU ball mill (equipped with ZrO_2 milling balls with abs. C_2H_5OH), and ball milled for 8 h. The obtained slurry was evaporated and dried at 353.15 K for 2 h and sieved with a 100-mesh grid. Next, 30 g of the product was weighed and loaded into a 50 mm graphite die. A graphite paper coated with BN powder and graphite gaskets were placed between the die and the powder samples.	Temp.: 573.15-2273.15 K	NA	The Si_3N_4 ceramic sample with 2 wt% MgO and 5 wt% Y_2O_3 presents the best properties such as bending strength: 1113 ± 92 MPa; fracture toughness: 8.39 ± 0.38 MPa $m^{1/2}$; hardness: 1837.7 ± 79.5 HV; dielectric loss: <0.01; dielectric constant: ~8.7.	NA	[89]
strontium-substituted lanthanum cobaltite ($La_{0.7}Sr_{0.3}CoO_{3-\delta}$, LSC)	Uniaxial die-pressing	NA	Firstly, La_2O_3 was pre-calcined at 1273.15 K for 2 h. Secondly, the desired amount of La_2O_3, $SrCO_3$, and Co_3O_4 were mixed for 8 h which is in accord with the stoichiometric ratio in $La_{0.7}Sr_{0.3}CoO_{3-\delta}$. Thereafter, the mixture was added and mixed with 15 wt.% starch in ethanol for 2 h, and then mixed with 3 wt.% PVB by grinding for 30 min. Finally, the mixture was dried and pressed into pellets at ~300 MPa using a stainless steel mold.	Temp.: 1373.15 K; Time: 12 h	Infiltration process of NiO NPs, followed by calcination	Average weight: were 0.15 g; diameter: 1.16 cm; thickness: 0.05 cm; Porosity: ~38.9%.	Electrochemical capacitors	[90]
α- Al_2O_3 supported mesoporous γ-Al_2O_3	Sol-gel route	Disk	NA	Temp.: 673.15 K; Time: 3 h; HR: 0.5 °C/min; CR: 0.5 °C/min	dip-coating with TiO_2/ZrO_2 sols	NA	Water treatment/ nanofiltration	[91]
α- Al_2O_3	Phase inversion	HFM	PVP, NMP, and PES were mixed and stirred at 343.15 K until a homogeneous solution is obtained. Then, Al_2O_3 powder was gradually added into the solution with continuous stirring. The dope solution was subsequently degassed at 343.15 K. Thereafter, a tube in orifice spinneret was used to get HF precursor with dope solution pressed by nitrogen gas at 1 bar.	Temp.: 1473.15–1873.15 K; Time: 2 h; HR: 1 °C/min	Deposition via IP of 1,3-diaminopropane and trimesoyl chloride	Mean pore size: ~0.28 μm. OD: 1.75 mm, ID: 1 mm.	Pervaporation	[92]
α-Al_2O_3	Phase inversion	HFM	PVP, NMP, and PES were mixed and stirred at 343.15 K until a homogeneous solution is obtained. Then, Al_2O_3 powder was gradually added into the solution with continuous stirring. The dope solution was subsequently degassed at 343.15 K. Thereafter, a tube in orifice spinneret was used to get HF precursor	Temp.: 1473.15–1873.15 K; Time: 2 h; HR: 1 °C/min	Coating with aluminum sol	Mean pore size: 229 nm.	Nanofiltration	[93]

Table 5 (*Continued*)

Ceramic	Fabrication method	Shape of components	Information on component preparation	Sintering parameters	Components modification	Properties of component/remarks	Application	Ref.
			with dope solution pressed by nitrogen gas at 1 bar.					
α-Al_2O_3	Phase inversion	HFM	Al_2O_3, SiO_2 or kaolin powder was introduced to PES/PVP/NMP solution, with mechanical stirring for at least 24 h. Then, the homogenous solution was degassed at a moderate temperature (343.15 K).	Temp.: 1473.15–1873.15 K; Time: 2 h; HR: 2 °C/min	NA	When sintering temperature was 1600 °C, Al_2O_3–kaolin (Al_2O_3: kaolin = 1:1) achieved a mean pore size: ~0.5 μm.	NA	[94]
BN-SiO_2	Cold isostatic pressing	Discs	SiO_2 and BN powders were mixed, ball milled for 4 h at a rate of 400 rpm in C_2H_5OH. The mixtures were subsequently dried at 373.15 K for 12 h. Finally, the powders were hot-pressed to Φ20 mm discs at 1673.15 -~1973.15 K at 30 MPa for 1 h under air atmosphere.	Temp.: 1673.15–1973.15 K; Time: 1 h	NA	The densest sample sintered at 1650°C with 50 wt% BN exhibits a relatively high thermal conductivity: 6.75 W/m K; a low dielectric constant: 3.73; and a low dielectric loss: 3.18×10^{-3}.	High frequency	[95]
Y-TZP	Extrusion	Tubular membrane	The ceramic slurry (132 g Y-TZP powder, 4 g APTES, 20 g PVA- H_2O solution (25 wt.%) and 13.5 g double-DI H_2O. The ingredients were milled, using 50 Al_2O_3 grinding balls at 350 rpm for 3 h while changing the rotation direction every 5 min. Thereafter, the slurry was shaped with a self-made laboratory extruder with an extrusion speed of 50 cm/min. Thereafter, dried for at least 48 h at room temperature, the capillaries were sintered at 1323.15 K for 2 h with dwell times at 553.15 K (0.5 h), and 773.15 K (1 h).	Temp.: 1323.15 K; Time: 2 h	Incubation in piranha solution (97 % H_2SO_4: 35% H_2O_2, 3:1 (v/v)) for 30 min	Log-reduction values: 0.3 ± 0.1–3.4 ± 0.2.	Virus filtration	[96]
Al_2O_3	Slip casting and powder compaction route/ uniaxial die-pressing	NA	For slip casting: to make carbon black slurries, solutions with varying PVP content were prepared. Then, ZrO_2 grinding media at a 2:1 ratio of ZrO_2 grinding media to carbon black powder was added to the PVP solutions. The carbon black powder was later added and milled at 60 rpm for 6 h. In slip casting route Al_2O_3/clay slurries were mixed at a later stage to make a ceramic-carbon composite. Al_2O_3 clay slurry with 26 vol.% solid content (65 wt% clay, 35 wt% Al_2O_3) was made in PVA solution (1 wt%). NaPAA (1 ml/100 gm of Al_2O_3/clay mix) and n-octanol (100 μl/100 gm of Al_2O_3/clay mix) were added to the PVA solution. ZrO_2 grinding media at 1:1 of grinding media to Al_2O_3/clay ratio was added and milled for ~24 h. Mixing of Al_2O_3/clay carbon black slurries was carried out in a polypropylene bottle on the pot mill. Carbon black slurries (2 to 7 wt.% carbon black with respect to Al_2O_3/clay mix) was added to Al_2O_3/clay slurries and mixed for 24 h. Ceramic carbon composites were made by casting the slurries in ring-shaped plastic molds on gypsum-mold base plates. The inner surface of the plastic molds was coated with WD40. Cast components were removed from the plastic molds after allowed to dry for 12 h in ambient condition. The green components were kept for 36 h in air, followed by drying in the oven for 5 days at	Temp.: 1673.15 K	NA	NA	NA	[97]

			323.15 K. For powder compaction route; Al_2O_3, graphite powder, carbon black and clay were dispersed in THF. These mixtures were mixed at 90 rpm for 5 days. Mixtures were removed and sieved. Elimination of THF by drying was done at 373.15 K in an oven. Pellets were made by compacting the mixtures in a uniaxial press at a load of 1.5 t.					
ZrO_2/ Al_2O_3 (ZTA) 20:80	Uniaxial die-pressing	blocks	NA	Temp.: 1073.15–1273.15 K	Vapor deposition of hydrogenated-carbon nitride film by pyrolysis of ethylenediamine at temp. of up to 1000 °C	NA	NA	[98]
a-SiC	Uniaxial die-pressing	Disk	NA	Temp.: 1423.15–1723.15 K; HR: 100 °C/min; CR: 20 °C/min; Time: 10 min	Diffusion bonded with a powder mixture of graphite, Si and TiH_2 by spark plasma sintering	NA	NA	[99]
β- Si_3N_4	Uniaxial die-pressing	Rectangular locks	NA	Temp.: 1023.15–1153.15 K; HR: 10−20 °C/min; CR: 5 °C/min; Time: 10 min	Brazing with TiAl alloy using an AgCu filler alloy	Porosity: 43 %	NA	[100]
α-Si_3N_4	UDP and cold isostatic pressing	Disks	Si_3N_4, Yb_2O_3-MgO, 5 mol% carbon at molar ratios 93:2.5:5 were mixed. The powder mixtures were ball milled in ethanol for 1 h using Si_3N_4 balls. After drying, crushing and sieving, the mixtures were uniaxially dry pressed in a steel die at ∼60 MPa into pellets of Ø20 mm × 5 mm, followed by cold isostatic pressing at 200 MPa. The green compacts were put into a BN crucible and embedded in BN packing powder in a BN crucible. The Si_3N_4 ceramic was obtained over a two-step gas pressure sintering process, including the first step for 8 h at 1773.15 K and a second step for 12 h at 2173.15 K under a nitrogen pressure of 1 MPa.	Two-step gas pressure sintering: Temp.: 1773.15 K; Time: 8 h Temp.: 2173.15 K; Time: 12 h under N_2	NA	The C-doped Si_3N_4 exhibited a considerably high thermal conductivity: 128 W.m.K, which showed a significant increase of ∼25.5% as compared to 102 W/m K for the un-doped Si_3N_4 component.	NA	[101]
α- Al_2O_3	Phase-inversion	HFM	CuO, Al_2O_3, and TiO_2 powders were added to the polymer solution (PSf, PVP and DMAC), and the mixture was milled for a day. The solution was composed of 0.5 wt% PVP, 49.25 wt.% DMAC, 7 wt% PSf, and 43.25 wt.% ceramic powder.	Temp.: 873.15–1523.15 K; HR: 2 °C/min; Time: 1-2 h	NA	Optimum membrane shows maximum flexural strength: 116.78 MPa; Porosity: 34.6%; Mean pore size: 700 nm; PWF: 1255 $Lm^{-2}\,h^{-1}$; degradation efficiency: 81.5%.	Catalytical activity	[102]
TiC	NA	Pellets	The TiC ceramics were formed by the combustion synthesis of titanium with carbon powder at 3273.15 K (mole ratio of Ti/C = 1).	NA	NA	Showed a nano-structural morphology with a high surface area, and electrical conductivity, and a photo-absorption at the Nd:YAG laser band: 355 nm.	Detection of environmental pollutants	[103]
Mullite-titania	Phase inversion	HFM	NA	NA	Dip coating with TiO_2 top-layer	NA	Wastewater treatment	[104]
α- Al_2O_3	Phase inversion	Tubular membrane	NA	NA	In situ chemical deposition	NA	Nanofiltration	[105]
α- Al_2O_3	Phase-inversion	HFM	NA	NA	NA	Stable hydrophobic character but very low flux.	Membrane distillation	[106]
Al_2O_3/mullite	Freeze casting without template	Cylindrical plates	100 g mullite and 50 g Al_2O_3 powder were added to 50 g SiO_2 sol. The slurry was homogenized, processed and dried analogous to the clay slurry with an increasing freezing	Temp.: 1673.15 K; Time: 2 h; HR: 2 K/min; CR: 5 K/min	NA	Lamellar pores. mean settlement rate: 46.2 %.	Aquaculture	[107]

Table 5 (*Continued*)

Ceramic	Fabrication method	Shape of components	Information on component preparation	Sintering parameters	Components modification	Properties of component/remarks	Application	Ref.
			time of 1 h, and a reduced drying period of 24 h.					
Al_2O_3/mullite	Freeze casting with template	Cylindrical plates	150 g SiO_2 sol was diluted with 30 g distilled H_2O and mixed with 300 g mullite powder, 150 g of Al_2O_3 powder, and 3.1 g PAA and homogenized for 16 h. The slurry was filled into a PVC mold and the dispersed surface was covered with polystyrene spheres as templates to produce large pores on component top. The mold was placed inside the freezer for 3 h at 123.15 K. After removal and de-molding of the casted plates were dried at room temp. and RH of 30 ± 5% for 48 h.	Temp.: 200–1823.15 K; Time: 2 h; HR: 0.5−2 K/min; CR: 5 K/min	NA	By the addition of spherical polystyrene beads during freeze casting (mullite-Al_2O_3), superficial pores in the size of the larvae were created, exhibiting significantly lowest survival rate of settlers of 79%.	Aquaculture	[107]
Al_2O_3	Direct foaming	Cylindrical plates	Firstly, homogeneous aqueous Al_2O_3 slurry with 0.74 wt.% of anionic polyelectrolyte dispersant and particle content of 42.5 vol% was prepared using a mixer for 20 min at a stirring velocity of 2500 rpm. Prior to emulsification at 10 kPa and stirring speed of 1100 rpm, the decane and anionic surfactant were added to reach concentrations of 70 vol% and 0.33 vol%, respectively. The final emulsion was subjected to ambient pressure and poured into molds. The components were dried at RT for 4 days and RH of 50%. After demolding, an additional 1 day drying step under pressure reduction from 10 to 2 kPa at RT was performed.	Temp.: 1673.15 K; Time: 2 h; HR: 2 K/min; CR: 3 K/min	NA	Porosities: 83 %; cellular pore types, mean settlement rate: 46.2 %.	Aquaculture	[107]
3Y-TZP	Uniaxial die-pressing	Blocks	NA	Temp.: 1173.15 K; Time: 2 h	Slip coating with HAP	NA	Biomedical	[108]
SiCO	Gel casting	Blocks	The porous SiCO ceramic composites were prepared through sol-gel, drying, and pyrolysis, using methyldimethoxysilane and methyltrimethoxysilane (precursors), NH_4OH and HNO_3 (catalysts), hard carbon felt (reinforcement) and EtOH (solvent). The prepared composites were hand-polished with 100-grit emery paper.	NA	Coating with $TaSi_2$-$MoSi_2$-ZrO_2-borosilicate glass	NA	Thermal insulation	[109]
8 mol% Y-TZP	Freeze casting	Thin film	Freezing of thin-film self-supported component sample occurs from bottom to top of the suspension. Suspensions were poured in a mold which had a Cu disc base and was covered with a polypropylene lid. Spacers of 500 μm thickness were placed between the Cu disc and the lid. The Cu disc was in contact with a metallic base, which was immersed in liquid nitrogen. Freeze casting of suspensions was done at two fixed rates: 1 °C/ min and 5 °C/min by cooling from RT to 243.15 K. Thereafter, they were introduced in the freeze dryer for > 3 h. The condenser temperature was set at 223.15 K.	Temp.: 1523.15 K; Time: 2 h; HR: 2 °C/min; CR: 2 °C/min	Electrolyte deposition, lamination and sintering	NA	NA	[110]

TiB_2 (98%) and -SiC (2%)	Uniaxial die-pressing	Tape	The mixture of TiB_2 and SiC was placed into a polyethylene jar, ball-milled at a speed of 325 rpm for 24 h (mass ratio of raw powder to WC balls was 1:10) with ethanol. The mixed powders were subsequently dried in a vacuum oven and sieved through a 100-mesh sieve. Next, the dried powder was filled into a graphite mold and pre-pressed at 10 MPa for 5 min. Finally, the ceramic body was sintered in a spark plasma sintering furnace with a uniaxial load of 30 MPa.	Temp.: 1873.15 K; Time: 5 min; HR: 100 °C/min	Laser-induced oxidation	NA	Thermal insulation	[56]
GDC-NiO	Uniaxial die-pressing	Thin film	Gd_2O_3 and CeO_2 were mixed in 1:9 proportion. The mixed powder was then calcined at 1473.15 K/4 h to prepare GDC powder. The GDC powder was then reground and mixed with NiO in the desired proportion to obtain the composite phase of NiO-GDC. The mixed powder was then again reground with PVA. The PVA added powder was pelletized with a hydraulic press machine.	Temp.: 1673.15 K; Time: 8 h	Reduction treatment in an atmosphere of 5% H_2-95% Ar with a gas flow rate of 500 ml/min for 5 h at 900 °C.	NA	NA	[111]
GDC-NiO	Uniaxial die-pressing	Thin film	Gd_2O_3 and CeO_2 were mixed in 1:9 proportion. The mixed powder was then calcined for 4 h at 1473.15 K, to prepare GDC powder. The GDC powder was then reground and mixed with NiO in the desired proportion to obtain the composite phase of NiO-GDC. The mixed powder was then again reground with PVA. The PVA added powder was pelletized with a hydraulic press machine.	Temp.: 1773.15 K; Time: 8 h	spray pyrolysis	NA	NA	[112]
$Bi_2Ge_3O_9$	Uniaxial die-pressing	Pellets	Bi_2O_3 and GeO_2 powders were batched and thoroughly mixed by the ball milling for 24 h. The mixed slurry was then dried, and the resulting powders were calcined for 5 h at 973.15 K. The calcined powders were subsequently ball-milled again for another 24 h and dried to obtain fine ceramic powders. Finally, these powders were uniaxially pressed into cylindrical pellets.	Temp.: 1123.15–1173.15 K; Time: 5–11 h	NA	Promising microwave dielectric properties for the advanced ceramic component (average grain size: 2.7 μm; εr: 9.7; τ_f: −29.5 ppm/°C and Q × f: 48,573 GHz).	Microwave	[113]
Li_2MgSiO_4	Uniaxial die-pressing	Pellets	Li_2CO_3, MgO, and SiO_2 were mixed using ZrO_2 balls and de-mineralized H_2O for 5 h. The resulting suspension was dried for 2 h at 373.15 K and then ground. This powder was calcined for 4 h at 1123.15 K. Finally, 1% PVA solution was added to the calcined powder, mixed, and grounded, and pressed into cylindrical pellets of ~18 mm in diameter and 5.9 mm in thickness, by applying a pressure of ~100 MPa.	Temp.: 1373.15 K; Time: 6 h	NA	Exhibited a relative permittivity (εr): 5.73; dielectric loss: 5.897×10^{-4} at 8 GHz.	Microwave	[114]
α- Al_2O_3	Phase inversion	HFM	Suspension solution was prepared by dissolving the additive in the DMSO followed by adding the required amount of Al_2O_3 powder. The solution was agitated for 48 h in a ball mill. The PES was subsequently added and the mixture was agitated for further 48 h.	Temp.: 1623.15 K; HR: 5 °C/min	Deposition with palladium	NA	Gas separation	[115]
AlON	Gel casting	Thin film	A homogeneous mixture of Al_2O_3 powder and carbon black (5.5% carbon), was sintered at 1993.15 K to obtain pure phase AlON powder. The synthetic powder was milled and refined	Temp.: 2193.15 K; Time: 10 h	Coating with VO_2 sol.	NA	Infrared and terahertz smart window	[116]

Table 5 (*Continued*)

Ceramic	Fabrication method	Shape of components	Information on component preparation	Sintering parameters	Components modification	Properties of component/remarks	Application	Ref.
			and then remained for 10 h under air at 973.15 K.					
$CaCoSi_2O_6$	Uniaxial die-pressing	NA	$CaCO_3$, $CoCO_3$, SiO_2 were weighted and then ball milled for 8 h in nylon containers with ZrO_2 balls and distilled H_2O. After dried at 383.15 K, the obtained powders were calcined for 2 h at 1373.15 K and ball-milled again for another 6 h and dried. The dried powders were then mixed with 15 wt% paraffin and sieved through a 60-mesh screen. Then, the powders were pressed into pellets with 7.5 mm in thickness and 15 mm in diameter.	Temp.: 1398.15–1473.15 K; Time: 2 h; HR: 5 °C/min	NA	The optimum microwave dielectric properties were obtained (εr: 6.04, $Q \times f_0$: 12457 GHz and τ_f: −18.91 ppm/°C).	Microwave dielectric	[117]
β-eucryptite	Uniaxial die-pressing	NA	$LiOH{\cdot}H_2O$, SiO_2 and $Al(OH)_3$ with 1:1:1 in the molar ratio were weighed and then mixed. The slurry was dried and then calcined for 2 h at 973.15 – 1223.15 K to prepare β-$LiAlSiO_4$ powders. The as-prepared β-$LiAlSiO_4$ powders were ball milled with DI H_2O. The slurry was dried and then granulated with a 10 wt.% PVA-H_2O solution. Thereafter, the granules were pressed into cylindrical green bodies, heat-treated at 773.15 K for 1 h.	Temp.: 1473.15 K; Time: 1−2 h; HR: 5 °C/min	NA	The β-$LiAlSiO_4$ ceramic sintered for 1 h at 1200 ℃ shows dense and less cracked microstructure with zero coefficient of thermal expansion α: -0.5×10^{-6}/K.	Thermal properties	[118]
$SrCeO_3$	Cold isostatic pressing	NA	The powders were compacted by CIP at 200 MPa to obtain green bodies.	Temp.: 1773.15 K; Time: 20 h	Coating with V_2O_5	NA	Electrical conductivity	[119]
β-Sialon	Phase inversion	HFM	The powder mixtures (-Si_3N, AlN, Al_2O_3, and Y_2O_3) were ball milled using high-purity Si_3N_4 media and methanol for 12 h, and subsequently dried and sieved through a 150 μm screen. The dispersant AMPG and PES were dissolved in NMP. Then the powder mixtures were added into the solution, followed by ball milling for 16 h.	NA	Immersion in 2 wt.% FAS in ethanol solution for 24 h and dried for 12 h at 100 °C.	NA	Membrane distillation	[120]
3Y-TZP	Freeze casting with templates	Tubes	Ceramic suspensions were prepared by mixing distilled H_2O with 3 wt.% PVA, 0.75 wt. % of dispersant (Prox B03), and 3 mol% Y-TZP. After a first mixing step with a magnetic stirrer, the slurry was ball milled at 800 rpm for a minimum of 18 h. Afterward, it was de-aired for 10 min and poured in a tubular mold. The slurry-filled tube was attached to the rotational clamp and the speed was set to 70 rpm. Silicon oil was pumped in the container with a preset temperature (243.15 or 193.15 K) until it achieved a steady flow. The system was left under rotational freezing of 5 min.	Temp.: 1673.15 K; Time: 3 h; HR: 5 °C/min; CR: 5 °C/min	NA	Decreasing pore volume and size increases the mechanical properties but decreases air permeability.	Gas separation	[121]
95 % Al_2O_3 and 5% SiO_2	Non-directional freeze casting	Fibers	Al_2O_3 fibers (95% Al_2O_3 and 5% SiO_2) with an average diameter of 3 μm were unglued by heat treatment for 1 h at 900 °C in air and then cut into short fibers by gently sliding them through a 900 μm test sieve. These fibers were gradually mixed with SiO_2 sol solution (DI H_2O, silica sol and PVA stirred at 343.15 K for 2 h) by ultrasonic dispersion for 1 h. The slurry-filled mold was immersed into liquid nitrogen (77.15 K) or place into a refrigerator	Temp.: 1623.15 K; Time: 3 h; HR: 5 °C/min	NA	The cooling temperature and slurry viscosity affected the dispersion of the particles rejected by the solidification front while the fiber length affected the fiber network. The material with optimal properties was obtained with 5 wt% silica sol, 5 wt% PVA, and 1 vol.% alumina fibers when freezing at −20 °C. The specific strength was 3.860 N m/kg and the bulk density was 199 kg/m^3.	NA	[38]

			at −20 °C for solidification. Freezing of the slurry was executed by pouring it into a cylindrical plastic mold (60 mm in height and 40 mm in diameter). Finally, sublimation was carried out by freeze-drying for 48 h at 223.15 K and 10 Pa.					
Fused silica	Freeze casting	Foam	Fused silica, fine Al_2O_3 and 0.05% CTAB were ball milled in H_2O using Al_2O_3 milling media in a 1:1 ratio for 100 h. This pre-treated powder mixture was further milled with sucrose (15 wt%) and binder (30 vol%), at 38 vol.% of solid loading. This suspension was subjected to the tumbling process for direct foaming by air entrapment. The slurries were poured into vaseline-coated aluminum molds cooled using liquid nitrogen for instant freezing. The frozen components were freeze-dried at low temperature (268.15 to 263.15 K) for 24 h. The freeze dryer was evacuated using a diffusion pump to a pressure range of 10^{-2} Torr.	Temp.: 1423.15 K; HR: 1 °C/min	NA	Density: 798 kg/m^3. Microstructural studies of the sintered foams have shown the presence of nearly spherical uniformly distributed pores with a size range of 50 to 175 μm. The larger pores are found to be interconnected through finer pores with ~15–25 μm. The pore size distribution in the freeze-cast foams is narrower.	NA	[39]
HAP/SiO_2	Freeze casting	Scaffolds	For slurry preparation, distilled H_2O was mixed with PAA and with colloidal SiO_2. pH was adjusted to 9–10 using NH_4OH. HAP powder was subsequently added, and the completed mixture was dispersed at 2300 rpm for 1 h. The ratio of ingredients was 50 wt % HAP powder and 50 wt% H_20 (including H_2O derived from added liquids). The slurry was filled into a metallic mold which was completely sealed and rapidly frozen in a deep freezer for 1.5 h at 423.15 K. After demolding, the components were dried slowly at 293.15 K for 4 h, at 277.15 – 281.15 K for 2 days, and a week at least in RT.	Temp.: 1373.15 K; Time: 4 h; HR: 4.4 K/min	NA	The addition of SiO_2 introduced a partial phase transformation of HA to β-tricalcium phosphate and improved the form stability due to less shrinkage after sintering. It also enhanced cell adhesion and proliferation.	Bone tissue engineering	[41]
Si_3N_4	Freeze casting	NA	For slurry preparation, Si_3N_4 powder, (Al_2O_3 and Y_2O_3), PVB solution, polyacrylamide, DI H_2O, and silicon nitride ball as raw material, composite sintering additives, binder, dispersant, solvent, and ball milling medium, respectively. The slurry was then placed in a vacuum defoamer to vacuum and remove bubbles. The vacuum defoaming slurry was frozen by freeze dryer at 13.33 Pa/233.15 K, and the slurry was frozen. Then the pressure was subsequently reduced to below 213.15 K /1.33 Pa. Finally, the freeze-dried porous silicon nitride body was sintered.	Temp.: 1623.15 K	NA	Porous Si_3N_4 structure with macro-directional growth and controllable pore structure. Show relatively uniform grain size when the diluent content was 30 wt.%. When Sm_2O_3 was used as a sintering additive, the bending strength of 300 MPa was reached.	NA	[122]
Mullite	Dry pressing	Disk	Bauxite and kaolin based on chemical compositions of mullite ($3Al_2O_3{\cdot}2SiO_2$) were ball-milled and mixed for 10 h at 300 rpm. The suspension was dried in the oven for 3 h at 373.15 K. Thereafter, the obtained powders were mixed with 1 wt.% PVA of total powders. The green membrane was produced by the dry-pressing under an applied pressure of 200 MPa.	Temp.: 1573–1873.15 K; HR: 3 °C/min before 1573.15 K and 2 °C/min after 1573.15 K; CR: 5 °C/min	NA	Membrane shows the highest open porosity (31.6 %) and good flexural strength of 100.2 MPa at a sintering temperature of 1500 °C.	NA	[123]
CCTO	Phase inversion	Hollow fiber	A pre-determined amount of CCTO powders were added into solution of PES, PVP and	NA	NA	Membrane presents higher photocatalytic efficiency when the content of CT particles	Wastewater treatment	[124,125]

Table 5 (*Continued*)

Ceramic	Fabrication method	Shape of components	Information on component preparation	Sintering parameters	Components modification	Properties of component/remarks	Application	Ref.
			DMAc. Subsequently the solution was used to spun the nascent fibers.			was 4 wt.% as compared to the pristine membrane.		
$Ca_2MgSi_2O_7:Ce^{3+}$ phosphor	NA	Plate	First, $CaCO_3$, MgO, SiO_2 and CeO_2 were comixed and homogenously ground with 10 at % H_3BO_3 for 30 min to produce as-prepared phosphor. Secondly, kaolin and $Ca_2MgSi_2O_7:Ce^{3+}$ phosphor was mixed and homogeneously grounded. The mixture was subsequently compressed into 1 cm diameter plate under pressure of 6 MPa. The powder mixtures were sintered via hot pressing sintering for 1 h at 1173.15 K.	NA	TiO_2 deposition	This substrate show suitable emission supporting photocatalysts for photocatalytic degradation of organic pollutants.	Wastewater treatment	[126]
Al_2O_3–TiO_2	Uniaxial press	Disc	α– Al_2O_3 and TiO_2 were homogenously mixed and ball milled using Si_3N_4 balls. Then, the mixture was uniaxially pressed at 100 MPa.	HR and CR: 5 °C/min, at 1573.15 K – 2 h or 1673.15 K – 2 h	Infiltration with lanthania containing glass at temperature of 1413.15 K -2 h	The ceramic components exhibit high density (94–99 % of theoretical density), fracture toughness (> 2.6 MPa $m^{1/2}$), fracture strength (218 ± 28 MPa - 254 ± 18 MPa) and Vickers hardness (895 ± 14–1036 ± 33 HV).	NA	[127]
BN-SiO_2	Hot press	Blocks	h-BN and amorphous SiO_2 powders were mixed to prepare the BN-SiO_2 ceramic	NA	NA	A good wettability with contact angles of ~44°–15° was achieved.	NA	[127]
Si_3N_4/TiC	Hot press	Blocks	Graphene was dispersed in PVP and IPA. TiC, Si_3N_4 were mixed in IPA by ultrasonic processing and mechanical agitation. After that, the mixed slurry was milled under nitrogen atmosphere for 42 h. Then, the dispersed graphene solution was added into the milled slurry and milled for another 6 h. The slurry was dried for 24 h in vacuum at 373.15 K and then sieved through a 200-mesh sieve. The powder mixtures were sintered via hot pressing sintering for 60 min at 1973.15 K under uniaxial pressure of 25 MPa.	NA	NA	The wear rate of 4.29×10^{-6} mm^3/N·m and friction coefficient of 0.46 which decreases by 63.0% and 31.3%, respectively.	NA	[128]
$MgAl_2O_4$ spinel	Direct foaming	Foams	Homogenous slurries containing 2 g rutile TiO_2 powders, 98 g spinel, and DI H_2O with solid content of 35 to 40 vol.%, methylene bisacrylamide, *N*-methacrylamide, and sodium hexametaphosphate were ball-milled for 2 to 3 h using Al_2O_3 balls with a ball-to-slurry mass ratio of 3:1. Lauryl alcohol, tetramethylethylenediamine, and SDS were then added in the suspensions, which were mixed vigorously to obtain the foamed slurries. Sodium carbocymethyl cellulose was slowly mixed in the foamed slurries. Finally, ammonium persulfate solution was quickly added into the foamed slurries and mixed rapidly. The foamed slurries were then immediately poured into plastic molds. After the in-situ polymerization of the foamed suspensions at ~298.15 K, 1 h aging, and demolding, green bodies were dried for 18 to 24 h at 323.15 K. Subsequently, the dried bodies were calcined at 2 °C/min to 873.15 K, and were soaked for 1 h before calcination in the range of 1473.15 to 1773.15 K for 2 h at 3 °C/min.	NA	NA	Pore size (10–200 μm), compressive strength (4.0–14.3 MPa), tailored porosity (75.14–82.46%), and dielectric constant (1.66–2.05).	NA	[129]

Si_3N_4-hBN	Hot pressing	Disc	Si_3N_4, h-BN, Al_2O_3 and Y_2O_3 were mixed by ball mill for 5 h at 500 rpm with ZrO_2 balls to ball ratio of 1:2. The mixed powders were formed by hot-press sinter at a pressure of 30 MPa for 30 min at 2073.15 K.	NA	NA	Under artificial seawater environment, wear rates and coefficients of friction of Si_3N_4-hBN sliding against poly-ether-ether-ketone decreases with increase of load. A COF value of 0.05 of and the wear rate value of 4.58×10^{-6} $mm^3/(N\,m)$.	Water treatment	[130]
$Li_{1.3}Al_{0.3}Ti_{1.7}(PO_4)_3$ (LATP)	Uniaxial press	Pellets	Li_2CO_3, $NH_4H_2PO_4$, TiO_2 and Al_2O_3 were mixed and annealed for 10 h at 1173.15 K to obtain the final compound. The as-prepared LATP was milled with lithium fluoride taken in molar ratio varying from 10 to 30 mol.%. Both powders were immersed in C_2H_5OH and ball milled for 1 h at 400 rpm. The obtained powder, after drying, was uniaxially pressed at 10 MPa.	NA	NA	The highest total ionic conductivity was obtained for ceramic sintered at 800 °C and was equal to a total resistance of 1.1×10^{-4} $S.cm^{-1}$.	Electronics	[131]
$BaAl_2Si_2O_8$	Uniaxial press	Pellets	$BaCO_3$, SiO_2, and Al_2O_3 were weighed and milled in distilled H_2O for 8 h using ZrO_2 balls. Subsequently, they were dried and calcined for 2.5 h at 1193.15 K. Li_2CO_3–B_2O_3 (molar ratio of B_2O_3 to Li_2CO_3 was 1:1) were added to the calcined $BaAl_2Si_2O_8$ powders, re-milled in distilled H_2O for 8 h. The obtained powder, after drying and sieving, was uniaxially pressed at 300 MPa.	Temp.:1123.15–1698.15 K for 3 h; HR: 3 °C/min	NA	The obtained ceramics show the good microwave dielectric properties of (ε_r): 6.34, ($Q \times f$): 24366 GHz, and (τ_f): −27.42 ppm/°C.	Electronics	[132]
Al_2O_3	NA	Disc	SiO_2, Al_2O_3, kaolin, $CaCO_3$, and Carbon powders were mixed and milled. The mixture was then ball milled, dried and compacted into ring-shaped component at 100 MPa for 1 min. The sample was sintered at the temperature of 1500 to 1873.15 K for 1 h.	NA	Metallization (deposition with Mo–Mn layer)	Tensile strength: 1990 ± 75 N, flexural strength: 9499 ± 346 N and a Helium leakage rate: 3.5×10^{-11} $Pa.m^3.s^{-1}$ were achieved for the optimized components after metallization.	Electronics	[133]
Si_3N_4	Hot press	Blocks	Si_3N_4 powders were grouped according to the concentration gradient and dispersed thoroughly with PTFE emulsion. An appropriate amount of deionized water is added. After 2 h, the mixed emulsion was placed at 303.15 K to evaporate to form a solid composite. The solid composite was then pulverized into powder and hot pressed under 20 MPa pressure at 653.15 K.	NA	NA	The Si_3N_4/PTFE composite exhibits relatively low water absorption (0.032%), high thermal conductivity (λ = 1.3 W/m K), low dielectric constant (ε_r = 4.03), and low dielectric loss (tan δ = 0.0014).	NA	[134]

ceramic material to realize a dielectric resonator antenna (DRA), the radiation efficiency can be enhanced due to absence of surface waves associated with DRA as well as low conductor and dielectric losses. The material requirements for component applications are chemical compatibility with electrode material, low temperature variation of dielectric constant, low dielectric constant (Qxf > 1000 and εr < 20), high thermal conductivity, and preferably low thermal expansion [136].

Using chemically synthesized ceramic powder materials like borides, carbides, oxides, and nitrides have been fabricated with tailored microstructures and characteristics (such as hole or electron charge carrier mobility, band gap) for electronic applications. A recent example of newly synthesized materials explored for electro-optic and semiconductor applications is binary nitrides with spinel (Ge_3N_4, Si_3N_4) and thorium phosphate (Zr_3N_4, Hf_3N_4) structures. Besides its high hardness, the novel nitride polymorphs of Si_3N_4 and Ge_3N_4 possess a direct band gap between 3–4 eV, which is comparable to the blue/UV light emitting diode materials based on Ga, In, and Al nitride [137]. The first such Si_3N_4 (cubic g-Si_3N_4) was synthesized under high pressure [138].

Electrical insulators are materials used in electrical equipment as insulators or insulation being their function to support or to separate electrical conductors without allowing current through themselves [139]. Their applications have increased in the last years due to demand in the technology. Electrical insulators made from ceramics are widely used in many microelectronic devices. Multi-fold insulator applications form part of home appliances or aerospace and automotive sector. Ceramic insulators are also used for high voltage applications, being one of the most important pieces used in power transmission and distribution lines between others [139,140]. The properties required for an insulator in this field of application are high dielectric strength, good dissipation of heat and mechanical properties, a low-loss factor as well as high resistivity. One of the main limitations of ceramic materials in high voltage applications is a dielectric breakdown, which prompts the loss of mechanical degradation and the material insulating properties. Dielectric strength for high tension electrical insulation is currently limited to 30 kV/mm and only natural mica insulators provide larger values in terms of dielectric strength [139,141]. Dielectric breakdown is related to charge trapping and scattering process in specific areas of the insulator material [139].

Another example of emerging ceramic semiconductors is SiC. This material has a band-gap of 3.2 eV, which is about three times as wide as that of silicon, corrosion and oxidation resistance at high temperatures, and excellent mechanical properties and thus allows the application of SiC ceramics in semiconductor devices used in power electronics. Its low intrinsic carrier concentration and a high electron velocity are other interesting characteristics of SiC.

One area where there has been a very rapid growth of the ceramic component is that of microwave applications. Microwave dielectric ceramics are functional materials usually operating in the millimeter-wave frequency region. They have received great attention due to growth in their use on the internet, mobile communication, satellite systems, local area networks, as well as defense and civilian-related applications. This leads to increasing demand for new ceramics with the most suitable properties in a particular frequency range [142]. For decades, medium-permittivity dielectric ceramic and temperature-stable ceramics have been used as resonators in filters for microwave communication due to high permittivity and very low dielectric loss. Therefore, ceramics with complex and simple perovskite structures like (Mg, Ca) TiO_3, $ZrTiO_4$, $BaTi_4O_9$, $BaZn_{1/3}Ta_{2/3}O_3$, Ca-TiO_3-$NdAlO_3$, $ZrTiO_4$-$ZnNb_2O_6$, $Ba(Co, Zn)_{1/3}Nb_{2/3}O_3$ are used for base station resonators, while $Ba_4Nd_{9.33}Ti_{18}O_{54}$-based components find application as receivers in digital televisions [143].

Micro electro-mechanical systems (MEMS) are devices that often involve transduction processes that couple radiant, electrical, mechanical, magnetic, thermal, and chemical processes [144]. For example, SiCO has been used in the MEMS preparation by using mixtures of polysiloxane polymers with a variety of passive (SiC, Al_2O_3, TiB_2) or active (Al, TiH_2, Ti) fillers. Under micromolding, the polymer melt is solidified by thermal or chemical crosslinking, and subsequently, the shaped components are pyrolyzed to the final component of MEMS. In the same way, silicon–carbon–oxynitride micro-igniter [145] and SiCO micro-gear components [146] have been developed recently using the polymer-ceramic transformation process.

Chemical sensing is an application where electronic or ionic conductivity of oxide-based ceramic components is utilized. The sensors are increasingly used in various range of consumer and industrial applications including metal casting, steel-making, power plants, public safety, airplanes, and automobiles. Many of these applications demand reliable and rugged sensors that can operate in harsh environments. This sensor is able to detect the presence of various gases (hydrocarbons, CO, NO_x, O_2, CO_2, and volatile organic compounds) for air quality monitoring and emission control, as well as early fire warning, hazardous chemicals and smoke in mass transportation systems and public places [147]. The oxygen sensor that is usually used in the vehicle for combustion and emission control, utilizes the Y-TZP.

The development of structural ceramics for high temperature applications has become an emerging area of research in the past few years. These ceramics must exhibit certain properties including resistance to creep deformation at interfaces, chemical stability, oxidation resistance, low volatility, thermal shock resistance and sufficient toughness at ambient temperature [148]. Some non-oxide ceramics components made from SiC, Si_3N_4 are promising for applications at high temperatures, but unlikely to operate above a temperature of 1773.15 K. Silicon-based ceramic component has shown great promise in next generation gas turbine engines. Although, they show rapid degradation in H_2O vapor atmosphere, due to the volatilization of the protective SiO_2 scale. Thus, the normally protective SiO_2 scale [149] can degrade severely by reaction with impurities like H_2O vapors or alkali salts [150]. However, the most promising approach to enhance the protection of these materials (in this application) from H_2O vapor attack has been the use of plasma-sprayed external environmental barrier coatings [151].

Components packaging used in power electronics requires efficient heat dissipation, where the copper attached to the ceramic component is used as the heat sink. The packaging also provides electrical contact to the outside world, and protection to the semiconductor chip from harmful chemical species and enabling the handling of the chip. Most of the ceramic components used in microelectronic packages are based on glass-ceramic, Al_2O_3, beryllia, zirconia, and magnesia. Al_2O_3 is a material with a high dielectric strength which provides good electrical insulation, while copper provides excellent heat sinking via its high thermal conductivity. The choice of Al_2O_3 as the material is not ideal because it has a higher CTE than silicon, a relatively high relative permittivity (dielectric constant) and a relatively low thermal conductivity, the former which can lead to high frequency signal loss [152]. For these reasons, ceramics that have great potential to replace Al_2O_3 like cordierite ($2MgO.2Al_2O_3.5SiO_2$), SiC, and AlN have been kept under active consideration over the years as a possible replacement for component materials [152]. Consideration in the use of alternative components requires the development of a robust and suitable joining technology to bond the components to the heat sink material, which in reality is likely to be either aluminum or copper.

Biomedical applications

Ceramic components have also found use in Biomedical applications such as in dental prosthesis, hip prostheses, biomedical sensors, and microsystems for implantable applications [153–157]. Since ceramic biomaterials are not exposed to high temperature environments, low temperature bonding technologies including the use of glass ionomer cements, zinc phosphate cements, and composite resin cements can be used for bonding to dental ceramics and have been widely used [158,159]. The use of ceramic components has found wider space in prostheses, including dental implants and orthopedic, due to their wear resistance, strength, biocompatibility, and a good combination of stability [160]. For example, tetragonal Al_2O_3 and ZrO_2 have been used as femoral heads in the replacements of the total hip. Al_2O_3 has a better thermal conductivity while $ZrOn_2$ (in the tetragonal form) has better toughness and strength. Recently, Al_2O_3–ZrO_2 ceramic composites were also explored for joint prostheses. This composite was synthesized by a new colloidal processing route, involving the stable suspension of high-purity Al_2O_3 in diluted solutions of zirconium alkoxide. Due to narrow grain size distribution and the small size of ZrO_2 nano-grains thereof, larger amounts of tetragonal ZrO_2 could be retained in the material and thus contributing to an improvement in fracture toughness. One application in which a purely mechanical fit is used is the attachment of ceramic femoral heads to femoral stems in the replacement of prosthetic hip [157]. Ceramics used for such purposes tend to be made either from ZTA or Al_2O_3 [157]. Early technologies used brazing, screwing and gluing [157], but since the mid-1970s, heads have been attached to stems by a Morse taper design [161].

Environmental applications

Ceramic membranes have attracted increasing attention, due to their higher permeable properties, excellent thermal and chemical properties, and extended lifetime, high surface area, thus demonstrating better performances in water treatment, turbidity removal, desalination, wastewater treatment, and other important industrial applications [75,162–165]. For environmental applications, membrane-based components are the more favorable as they are fast and cost-effective, flexible to be integrated with other processes, and highly selective [166]. Ceramic membranes are usually comprised of the top-layer plus intermediate layer and the support [167,168] and hence, show high bending strength and permeability. During their applications, the ceramic support provides mechanical strength to a membrane active-layer (or top layer) to withstand the stress induced by the pressure difference applied over the entire membrane and simultaneously has a low resistance to the filtrate flow, while the intermediate layer prevents the penetration phenomenon. Most of the ceramic membrane supports are being fabricated from particles of ceramic oxides including Al_2O_3, TiO_2, SiO_2, and ZrO_2 [20,169]. Ceramic membranes made from Al_2O_3, ZrO_2, and TiO_2 have some unique advantages such as excellent mechanical strength, long life, superior chemical stability, and large surface area [170], which make them ideal components. Ceramic membranes are resistant to harsh environmental conditions due to their higher chemical stability, the aggressive chemical cleaning strategy could be used to control fouling [171,172]. Ceramic membranes for environmental applications are found mainly in the single-tube, multi-channel, flat and hollow fiber (HF) configurations. Among these, the multichannel ceramic membranes are mostly used, especially in industrial applications, due to their excellent mechanical strength and high packing density [173].

Solid oxide fuel cells are energy conversion systems in which fuels such as hydrogen or hydrocarbons react with air to generate a DC electrical current. The chemical reaction occurs through a ceramic membrane (ZrO_2) and involves ionic conduction of oxygen through the ZrO_2 electrolyte [161]. To achieve adequate electrical conductivity, the fuel cell must operate at 973.15–1173.15 K and should in addition offer low-gas leakage or preferably gas-tight. For these reasons, the application of ceramic component made of different components of the fuel cell is of often used and are of critical importance.

Conclusion and future outlook

In conclusion, alumina, boron, titanium, silicon, zirconia, and their nitrides derivatives are promising materials to produce ceramics components. Several synthetic methods for preparing ceramic components were elucidated. The solid-state reactions are the most widely used processes for the mass-production of cost-efficient ceramic powders. Also, the sol–gel technique, CVD, and polymer pyrolysis have been applied to generate high-purity ceramics precursor with defined properties. However, ZTA powders prepared via multiphase suspension mixing and sol-gel method have shown that 3Y-TZP have problems of abnormal grain growth with non-uniform distribution of grains and thermal aging. Hence, further studies are required to produce task-specific ZTA with improved morphology and microstructure. In general, the composite ceramic component offers several appealing and improved options compared to single crystal ceramics because of their high temperature and chemical stability, hardness, and wear resistance. The combination of these materials in molar percentage and the fabrication conditions results in different crystal phases with variant properties. Fabrication methods such as wet forming, slip casting, extrusion, powder injection molding, freeze casting, tape casting and cold isostatic pressing can be used to produce ceramics of various shapes and dimensions (HF, tubes and flat discs). Sintering temperature during fabrication mainly contributes to the transition in crystal phases, densification, and porosity of the ceramics. These properties impel characteristics such as hardness, corrosion-resistant, good conductivity, and microwave absorption on the ceramics. Machining is utilized to evolve ceramics with the desired shape, finish, strength, and size. However, most conventional machining constitutes about 60%–80% of the manufacturing cost of ceramics. In this review, solid freeform fabrication or temperature-induced forming is an alternative to obtained finished ceramics without defects. Particularly, 3-D printing is gaining increasing attention with greater prospects of large-scale commercialization. Furthermore, vast application channels of ceramics in biomedical, environmental and electrical renders it an attractive material. Ceramics application in power electronics is an emerging technology with interesting potentials of use in high temperature cycling because they are characterized by lower switching loss and higher voltage breakdown. Also, they provide a conducting path with relatively low resistivity, a thermal path towards heat sink and insulation effects between circuit and heat sinks.

Declaration of interests

The authors declare that they have no known competing financial interests or personal relationships that could have appeared to influence the work reported in this paper.

Acknowledgments

The first author acknowledges the financial support provided by the Shenyang University of Technology under the postdoctoral scheme. The authors also acknowledge the support of the Instituto de Energías Renovables (IER-UNAM), Universidad Nacional Autónoma de México, Key Laboratory for Catalyst Synthesis Technology of Polymer of Liaoning Province, China (No. 2010-36) and the

Engineering Laboratory for Advanced Polymer Material of Liaoning Province, China (No. 2012-1139).

References

[1] Y. Lv, H. Liu, Z. Wang, S. Liu, L. Hao, Y. Sang, D. Liu, J. Wang, R.I. Boughton, J. Membr. Sci. 331 (1) (2009) 50, doi:http://dx.doi.org/10.1016/j.memsci.2009.01.007.
[2] Y. Liu, H. Ma, B.S. Hsiao, B. Chu, A.H. Tsou, Polymer (Guildf). 107 (2016) 163, doi:http://dx.doi.org/10.1016/j.polymer.2016.11.020.
[3] H.W. Hennicke, A. Hesse, Traditional Ceramics, Pergamon, Oxford, 1991 488 pp.
[4] E. Horvath-Bordon, R. Riedel, A. Zerr, P.F. McMillan, G. Auffermann, Y. Prots, W. Bronger, R. Kniep, P. Kroll, Chem. Soc. Rev. 35 (10) (2006) 987, doi:http://dx.doi.org/10.1039/B517778M.
[5] A. Zerr, R. Riedel, T. Sekine, J.E. Lowther, W.Y. Ching, I. Tanaka, Adv. Mater. 18 (22) (2006) 2933, doi:http://dx.doi.org/10.1002/adma.200501872.
[6] M.V.J. Subrahmanyam, Mater. Sci. 27 (1992) 6249.
[7] A.G. Merzhanov, I.P. Borovinskaya, Dokl. Akad. Nauk SSSR, Seriya Khimiya 204 (2) (1972) 366.
[8] Ralf Riedel, I.-Wei Chen, Modern Trends in Advanced Ceramics, WILEY-VCH, Verlag GmbH, Weinheim, 2008.
[9] A. Terpstra, R.A. Pex, Petrus de Vries, Ceramic Processing, Springer, Netherlands, 2012.
[10] G.N. Howatt, R.G. Breckenridge, J.M. Brownlow, J. Am. Ceram. Soc. 30 (2006) 237.
[11] C. Ma, F. Tang, J. Zhu, M. Du, X. Yuan, Y. Yu, K. Wang, Z. Wen, J. Zhang, J. Long, W. Guo, Y. Cao, J. Am. Ceram. Soc. 99 (10) (2016) 3267, doi:http://dx.doi.org/10.1111/jace.14322.
[12] Y. Yang, Y. Wu, J. Mater. Res. 29 (19) (2014) 2312, doi:http://dx.doi.org/10.1557/jmr.2014.225.
[13] Z. Jingxian, J. Dongliang, L. Weisensel, P. Greil, J. Eur. Ceram. Soc. 24 (1) (2004) 147, doi:http://dx.doi.org/10.1016/S0955-2219(03)00340-6.
[14] Marc J. Madou, Fundamentals of Microfabrication: The Science of Miniaturization, 2nd ed., CRC Press, New York, 2002.
[15] Andrew Ruys, Alum. Ceram. (2019) 71.
[16] P.S. Monash Purushothaman, Gopal Pugazhenthi, Rev. Chem. Eng. (2013) 357, doi:http://dx.doi.org/10.1515/revce-2013-0006.
[17] A.R. Studart, U.T. Gonzenbach, E. Tervoort, L.J. Gauckler, J. Am. Ceram. Soc. 89 (6) (2006) 1771, doi:http://dx.doi.org/10.1111/j.1551-2916.2006.01044.x.
[18] J.A. Escribano, J. García-fayos, J.M. Serra, J. Eur. Ceram. Soc. 37 (16) (2017) 5223, doi:http://dx.doi.org/10.1016/j.jeurceramsoc.2017.05.032.
[19] A.R. Studart, E. Amstad, L.J. Gauckler, Langmuir 23 (3) (2007) 1081, doi:http://dx.doi.org/10.1021/la062042s.
[20] S.K. Hubadillah, M.H.D. Othman, T. Matsuura, A.F. Ismail, M.A. Rahman, Z. Harun, J. Jaafar, M. Nomura, Ceram. Int. 44 (5) (2018) 4538, doi:http://dx.doi.org/10.1016/j.ceramint.2017.12.215.
[21] S. Wardell, Slipcasting, University of Pennsylvania Press, 2007.
[22] K.K. Mallick, J. Winnett, Bone Substit. Biomater. (2014) 118 (Chapter 6).
[23] K.T. Faber, N.O. Shanti, Ceram. Compos. Process. Methods (2012), doi:http://dx.doi.org/10.1002/9781118176665.ch6.
[24] S. Barg, C. Soltmann, M. Andrade, D. Koch, G. Grathwohl, J. Am. Ceram. Soc. 91 (9) (2008) 2823, doi:http://dx.doi.org/10.1111/j.1551-2916.2008.02553.x.
[25] A. Imhof, D. Pine, Nature 389 (1997) 948, doi:http://dx.doi.org/10.1038/40105.
[26] S. Barg, E.G. de Moraes, D. Koch, G. Grathwohl, J. Eur. Ceram. Soc. 29 (12) (2009) 2439, doi:http://dx.doi.org/10.1016/j.jeurceramsoc.2009.02.003.
[27] I. Akartuna, A. Studart, E. Tervoort, L. Gauckler, Adv. Mater. 20 (24) (2008) 4714, doi:http://dx.doi.org/10.1002/adma.200801888.
[28] S. Kroll, C. Soltmann, D. Koch, P. Kegler, A. Kunzmann, Ceram. Int. 40 (10) (2014) 15763, doi:http://dx.doi.org/10.1016/j.ceramint.2014.07.100.
[29] R. Liu, T. Xu, C. Wang, Ceram. Int. 42 (2, Part B) (2016) 2907, doi:http://dx.doi.org/10.1016/j.ceramint.2015.10.148.
[30] K.L. Scotti, D.C. Dunand, Prog. Mater. Sci. 94 (2018) 243, doi:http://dx.doi.org/10.1016/j.pmatsci.2018.01.001.
[31] S. Deville, Adv. Eng. Mater. 10 (2008) 155, doi:http://dx.doi.org/10.1002/adem.200700270.
[32] Y. Du, N. Hedayat, D. Panthi, H. Ilkhani, B.J. Emley, T. Woodson, Materialia 1 (2018) 198, doi:http://dx.doi.org/10.1016/j.mtla.2018.07.005.
[33] J. Wettlaufer, M. GRAE WORSTER, H. Huppert, J. Fluid Mech. 344 (1997) 291, doi:http://dx.doi.org/10.1017/S0022112097006022.
[34] J. Zou, Y. Zhang, R. Li, Int. J. Appl. Ceram. Technol. 8 (2009) 482, doi:http://dx.doi.org/10.1111/j.1744-7402.2009.02458.x.
[35] Y. Chino, D.C. Dunand, Acta Mater. 56 (1) (2008) 105, doi:http://dx.doi.org/10.1016/j.actamat.2007.09.002.
[36] C. Stolze, T. Janoschka, U.S. Schubert, F. Müller, S. Flauder, Adv. Eng. Mater. 18 (1) (2015) 111, doi:http://dx.doi.org/10.1002/adem.201500235.
[37] S.L. Sobolev, Phys. Lett. A 376 (47) (2012) 3563, doi:http://dx.doi.org/10.1016/j.physleta.2012.10.031.
[38] X. Hu, L. Yang, L. Li, D. Xie, H. Du, J. Eur. Ceram. Soc. 36 (16) (2016) 4147, doi:http://dx.doi.org/10.1016/j.jeurceramsoc.2016.05.049.
[39] J. Verma, M. Vijayakumar, R. Mitra, Mater. Lett. 153 (2015) 168, doi:http://dx.doi.org/10.1016/j.matlet.2015.04.019.
[40] K. Mallick, J. Winnett, A. Bandyopadhyay, J. Am. Ceram. Soc. 95 (9) (2012) 2680, doi:http://dx.doi.org/10.1111/j.1551-2916.2012.05071.x.
[41] S. Blindow, M. Pulkin, D. Koch, G. Grathwohl, K. Rezwan, Adv. Eng. Mater. 11 (11) (2009) 875–884, doi:http://dx.doi.org/10.1002/adem.200900208.
[42] T. Krause, A. Molotnikov, M. Carlesso, J. Rente, K. Rezwan, Y. Estrin, D. Koch, Adv. Eng. Mater. 14 (5) (2012) 335, doi:http://dx.doi.org/10.1002/adem.201100244.
[43] F. Liu, N.A. Hashim, Y. Liu, M.R.M. Abed, K. Li, J. Membr. Sci. 375 (2011) 1, doi:http://dx.doi.org/10.1016/j.memsci.2011.03.014.
[44] T.A. Otitoju, A.L. Ahmad, B.S. Ooi, J. Polym. Res. 24 (8) (2017) 1, doi:http://dx.doi.org/10.1007/s10965-017-1268-6.
[45] A.L. Ahmad, T.A. Otitoju, B.S. Ooi, J. Taiwan Inst, Chem. Eng. 93 (2018) 461, doi:http://dx.doi.org/10.1016/j.jtice.2018.08.021.
[46] E. Klein, J.K. Smith, Prod. R&D 11 (2) (1972) 207, doi:http://dx.doi.org/10.1021/i360042a017.
[47] J. Luyten, A. Buekenhoudt, W. Adriansens, J. Cooymans, H. Weyten, F. Servaes, R. Leysen, Solid State Ionics 135 (1) (2000) 637, doi:http://dx.doi.org/10.1016/S0167-2738(00)00425-2.
[48] Z. Zhu, J. Xiao, W. He, T. Wang, Z. Wei, Y. Dong, J. Eur. Ceram. Soc. 35 (11) (2015) 3187, doi:http://dx.doi.org/10.1016/j.jeurceramsoc.2015.04.026.
[49] T.A. Otitoju, B.S. Ooi, A.L. Ahmad, React. Funct. Polym. 136 (2019) 107, doi:http://dx.doi.org/10.1016/j.reactfunctpolym.2018.12.018.
[50] J.M. Mánuel, F.M. Morales, R. García, T. Lim, L. Kirste, R. Aidam, O. Ambacher, Cryst. Growth Des. 11 (6) (2011) 2588, doi:http://dx.doi.org/10.1021/cg200341z.
[51] J.J. Jiménez, J.M. Mánuel, H. Bartsch, J. Breiling, R. García, H.O. Jacobs, J. Müller, J. Pezoldt, F.M. Morales, Ceram. Int. 45 (2019) 9114.
[52] K.M. Sree Manu, T.P.D. Rajan, B.C. Pai, J. Alloys Compd. 688 (2016) 489, doi:http://dx.doi.org/10.1016/j.jallcom.2016.07.135.
[53] M.T. Sebastian, H. Jantunen, in: M.T. Sebastian, R. Ubic, H. Jantunen (Eds.), Microwave Materials and Applications, Wiely Online, 2017, pp. 355.
[54] D.E. Clark, W.H. Sutton, Annu. Rev. Mater. Sci. 26 (1) (1996) 299, doi:http://dx.doi.org/10.1146/annurev.ms.26.080196.001503.
[55] J. Wang, B. Shen, L. Song, K. Zhu, J. Qiu, J. Alloys Compd. 762 (2018) 574.
[56] M. Wang, G. Zhao, N. He, L. Ma, L. Li, Ceram. Int. (2019).
[57] Z.J. Shen, M. Nygren, Key Eng. Mater. 206–213 (2001) 2155, doi:http://dx.doi.org/10.4028/www.scientific.net/KEM.206-213.2155.
[58] Z. Shen, M. Johnsson, Z. Zhao, M. Nygren, J. Am. Ceram. Soc. 85 (8) (2002) 1921, doi:http://dx.doi.org/10.1111/j.1151-2916.2002.tb00381.x.
[59] T.J. Goodwin, S.H. Yoo, P. Matteazzi, J.R. Groza, Nanostruct. Mater. 8 (5) (1997) 559, doi:http://dx.doi.org/10.1016/S0965-9773(97)00194-3.
[60] Toshiro Doi Eckart Uhlmann Ioan D, Marinescu, Handbook of Ceramic Grinding and Polishing, Elsevier, 2014.
[61] H. Peng, Z.J. Shen, M. Nygren, Key Eng. Mater. 206–213 (2001) 1121 10.4028/www.scientific.net/KEM.206-213.1121.
[62] L. Wang, F. Aldinger, Adv. Eng. Mater. 2 (3) (2000) 110 10.1002/(SICI)1527-2648(200003)2:3<110::AID-ADEM110>3.0.CO;2-4.
[63] R. Mutsuddy, B.C. Ford, Ceramic Injection Molding, Springer, 1994.
[64] N. Wang, D.P. Wang, Z.W. Yang, Y. Wang, X.G. Liu, Ceram. Int. 43 (13) (2017) 9636, doi:http://dx.doi.org/10.1016/j.ceramint.2017.04.133.
[65] Q. Dong, T. Zhu, Z. Xie, Y. Han, D. An, Ceram. Int. 43 (2017) 16943, doi:http://dx.doi.org/10.1016/j.ceramint.2017.09.099.
[66] W. Wesseling, S. Wittka, S. Kroll, C. Soltmann, P. Kegler, A. Kunzmann, H. Wolfgang, M. Lohmeyer, Aquaculture 446 (2015) 57–66, doi:http://dx.doi.org/10.1016/j.aquaculture.2015.04.017.
[67] I. Miccoli, R. Spampinato, F. Marzo, P. Prete, N. Lovergine, Appl. Surf. Sci. 313 (2014) 418, doi:http://dx.doi.org/10.1016/j.apsusc.2014.05.225.
[68] Y. Shi, L. Zhang, Z. Yue, Ceram. Int. 41 (2015) S504, doi:http://dx.doi.org/10.1016/j.ceramint.2015.03.298.
[69] S. Zhang, Y. Du, H. Jiang, Y. Liu, R. Chen, Ceram. Int. 43 (9) (2017) 7261, doi:http://dx.doi.org/10.1016/j.ceramint.2017.03.019.
[70] V.D. Phadtare, V.G. Parale, G.K. Kulkarni, H. Park, V.R. Puri, Ceram. Int. 44 (7) (2018) 7515, doi:http://dx.doi.org/10.1016/j.ceramint.2018.01.150.
[71] E. David, J. Kopac, Int. J. Hydrogen Energy 36 (7) (2011) 4498, doi:http://dx.doi.org/10.1016/j.ijhydene.2010.12.032.
[72] R. Shang, A. Goulas, C.Y. Tang, X. De Frias, L.C. Rietveld, S.G.J. Heijman, J. Membr. Sci. 528 (2017) 163, doi:http://dx.doi.org/10.1016/j.memsci.2017.01.023.
[73] S.A. Leonardi, M.A. Zanuttini, E.E. Miró, V.G. Milt, Chem. Eng. J. 317 (2017) 394, doi:http://dx.doi.org/10.1016/j.cej.2017.02.013.
[74] H. Yang, P. Liu, F. Yan, Y. Lin, T. Wang, J. Alloys Compd. 773 (2019) 244.
[75] C.-Y. Huang, C.-C. Ko, L.-H. Chen, C.-T. Huang, K.-L. Tung, Y.-C. Liao, Sep. Purif. Technol. 198 (2018) 79, doi:http://dx.doi.org/10.1016/j.seppur.2016.12.037.
[76] C.F. Xing, J. Bao, Y.F. Sun, J.J. Sun, H.T. Wu, J. Alloys Compd. 782 (2019) 754.
[77] N. Gao, Z. Xu, Sep. Purif. Technol 212 (November) (2019) 737.
[78] G. LI, H. QI, Y. FAN, N. XU, Ceram. Int. 35 (4) (2009) 1641, doi:http://dx.doi.org/10.1016/j.ceramint.2008.09.008.
[79] Z. Qu, Q. Zhang, R. He, Y. Pei, D. Fang, Ceram. Int 43 (November) (2017) 4399.
[80] H.Y. Chen, X.C. Wang, L. Fu, M.Y. Feng, Vacuum 156 (July) (2018) 256, doi:http://dx.doi.org/10.1016/j.vacuum.2018.07.043.
[81] M.G. Holthaus, L. Treccani, K. Rezwan, J. Eur, Ceram. Soc. 31 (2011) 2809, doi:http://dx.doi.org/10.1016/j.jeurceramsoc.2011.07.020.
[82] V.V. Tomina, N.V. Stolyarchuk, I.V. Melnyk, Y.L. Zub, T.F. Kouznetsova, V.G. Prozorovich, A.I. Ivanets, Sep. Purif. Technol. 175 (2017) 391.
[83] S. Danwittayakul, J. Dutta, J. Alloys Compd. 586 (2014) 169.
[84] Z. Feng, J. Qi, Y. Han, T. Lu, Ceram. Int. 44 (2018) 1059.
[85] Z. Sun, W. Li, Y. Liu, H. Zhang, D. Zhu, H. Sun, C. Hu, S. Chen, Ceram. Int. 45 (6) (2019) 7001, doi:http://dx.doi.org/10.1016/j.ceramint.2018.12.201.
[86] H. Lin, J. Niu, S. Liang, C. Wang, Y. Wang, F. Jin, Q. Luo, Chem. Eng. J. 354 (2018) 1058.
[87] P. Ninz, F. Kern, E. Ermantraut, H. Müller, W. Eberhardt, Procedia CIRP 68 (2018) 772, doi:http://dx.doi.org/10.1016/j.procir.2017.12.037.

[88] J. Yu, F. Yu, S. Wang, J. Zhang, F. Fan, Q. Long, Ceram. Int. 44 (2018) 17630.
[89] W. Liu, W. Tong, R. He, H. Wu, S. Wu, Ceram. Int. 42 (2016) 18641.
[90] P. Liu, Z. Liu, P. Wu, X. Ou, Y. Zhang, Int. J. Hydrogen Energy (2018) 1.
[91] H. Guo, S. Zhao, X. Wu, H. Qi, Microporous Mesoporous Mater. (2016), doi:http://dx.doi.org/10.1016/j.micromeso.2016.03.011.
[92] X. Liu, Y. Cao, Y. Li, Z. Xu, Z. Li, M. Wang, X. Ma, J. Membr. Sci. 576 (2019) 26.
[93] Z. Wang, Y.-M. Wei, Z.-L. Xu, Y. Cao, Z.-Q. Dong, X.-L. Shi, J. Membr. Sci. 503 (2016) 69, doi:http://dx.doi.org/10.1016/j.memsci.2015.12.039.
[94] L.F. Han, Z.L. Xu, Y. Cao, Y.M. Wei, H.T. Xu, J. Membr. Sci 372 (1–2) (2011) 154, doi:http://dx.doi.org/10.1016/j.memsci.2011.01.065.
[95] L. Wu, F. Xiang, W. Liu, R. Ma, H. Wang, Ceram. Int. 44 (2018) 16594.
[96] J. Bartels, A.G. Batista, S. Kroll, M. Maas, K. Rezwan, J. Membr. Sci. 571 (2019) 85.
[97] R. Kumar, P. Bhargava, J. Asian Ceram. Soc. 5 (2017) 304.
[98] J. Guo, J. Zhang, L. Yu, Z. Wu, Z. Zhang, Thin Solid Films 542 (2013) 60.
[99] Z. Wang, H. Li, Z. Zhong, A. Yang, C. Chen, K. Song, Y. Wu, J. Alloys Compd. 763 (2018) 875, doi:http://dx.doi.org/10.1016/j.jallcom.2018.06.013.
[100] Y. Zhao, X. Song, S. Hu, J. Zhang, J. Cao, W. Fu, Ceram. Int. 43 (March) (2017) 9738.
[101] J. Ko, Y. Park, Z. Huang, J. Eur. Ceram. Soc. 39 (2018) 157, doi:http://dx.doi.org/10.1016/j.jeurceramsoc.2018.10.006.
[102] S. Wang, J. Tian, Q. Wang, Z. Zhao, F. Cui, G. Li, J. Membr. Sci. 571 (2019) 333.
[103] H. Moriwaki, T. Otsuka, Y. Kawabe, I. Osaka, A. Miyazato, Int. J. Mass Spectrom. 428 (2018) 49, doi:http://dx.doi.org/10.1016/j.ijms.2018.02.008.
[104] L. Zhu, M. Chen, Y. Dong, C.Y. Tang, A. Huang, L. Li, Water Res. 90 (2016) 277, doi:http://dx.doi.org/10.1016/j.watres.2015.12.035.
[105] X. Chen, Y. Zhang, J. Tang, M. Qiu, K. Fu, Y. Fan, J. Membr, Sci. J. 552 (February) (2018) 77.
[106] C. Ko, A. Ali, E. Drioli, K. Tung, C. Chen, Y. Chen, F. Macedonio, Desalination 440 (2018) 48.
[107] M.M. Hoog, L. Röpke, J. Bartels, C. Soltmann, A. Kunzmann, K. Rezwan, S. Kroll, Ceram. Int. 44 (2018) 16561.
[108] J. Yang, R. Sultana, X. Hu, Z. Huang, J. Eur. Ceram. Soc. 31 (2011) 2065, doi:http://dx.doi.org/10.1016/j.jeurceramsoc.2011.05.025.
[109] X. Li, J. Feng, Y. Jiang, H. Lin, J. Feng, Ceram. Trans. 44 (May) (2018) 19143.
[110] J. Gurauskis, C.R. Graves, R. Moreno, M.I. Nieto, J. Eur. Ceram. Soc. 37 (2017) 697.
[111] M.G. Chourashiya, L.D. Jadhav, Int. J. Hydrogen Energy 36 (2011) 14984, doi:http://dx.doi.org/10.1016/j.ijhydene.2010.12.083.
[112] M.G. Chourashiya, S.R. Bharadwaj, L.D. Jadhav, Thin Solid Films 519 (2010) 650, doi:http://dx.doi.org/10.1016/j.tsf.2010.08.110.
[113] X. Ma, S. Kweon, S. Nahm, C. Kang, S. Yoon, Y. Kim, J. Eur. Ceram. Soc. 37 (2017) 605.
[114] A. Rose, B. Masin, H. Sreemoolanadhan, K. Ashok, T. Vijayakumar, Appl. Surf. Sci. 449 (2018) 96.
[115] M. Terra, L.P. Bessa, V.L. Cardoso, M. Hespanhol, M. Reis, Int. J. Hydrogen Energy (2017) 1, doi:http://dx.doi.org/10.1016/j.ijhydene.2017.10.179.
[116] B. Peng, Q. Shi, W. Huang, S. Wang, J. Qi, T. Lu, Ceram. Int. 44 (April) (2018) 13674.
[117] M. Xiao, Y. Wei, P. Zhang, Mater. Chem. Phys. 225 (2019) 99, doi:http://dx.doi.org/10.1016/j.matchemphys.2018.12.027.
[118] A.X. Yao, Y. Zhang, H. Ren, H. Peng, J. Eur, Ceram. Soc. 39 (2018) 1564, doi:http://dx.doi.org/10.1016/j.jeurceramsoc.2018.11.014.
[119] J. Yuan, H. Zhang, X. Zhou, J. Sun, J. Wang, S. Dong, J. Jiang, L. Deng, X. Cao, Corros. Sci. 145 (2018) 295, doi:http://dx.doi.org/10.1016/j.corsci.2018.10.013.
[120] J.-W. Wang, L. Li, J.-W. Zhang, X. Xu, C.-S. Chen, J. Eur, Ceram. Soc. 36 (1) (2016) 59, doi:http://dx.doi.org/10.1016/j.jeurceramsoc.2015.09.027.
[121] J. Seuba, J. Leloup, S. Richaud, S. Deville, C. Guizard, A.J. Stevenson, J. Eur, Ceram. Soc. 37 (6) (2017) 2423, doi:http://dx.doi.org/10.1016/j.jeurceramsoc.2017.01.014.
[122] C. Xiao, B. Han, J. Mater, Res. Technol. 8 (6) (2019) 6202, doi:http://dx.doi.org/10.1016/j.jmrt.2019.10.014.
[123] Z. Zhu, Z. Wei, W. Sun, J. Hou, B. He, Y. Dong, Appl. Clay Sci. 120 (2016) 135, doi:http://dx.doi.org/10.1016/j.clay.2015.11.020.
[124] T.A. Otitoju, D. Jiang, Y. Ouyang, M.A.M. Elamin, S. Li, J. Ind. Eng. Chem. 83 (2020) 145, doi:http://dx.doi.org/10.1016/j.jiec.2019.11.022.
[125] T.A. Otitoju, Y. Li, R. Liu, J. Wang, Y. Ouyang, D. Jiang, S. Li, J. Water Process Eng. 33 (August) (2020)101072, doi:http://dx.doi.org/10.1016/j.jwpe.2019.101072.
[126] H. Sun, H. Wu, Y. Jin, Y. Lv, G. Ju, L. Chen, Z. Feng, Y. Hu, Mater. Lett. 240 (2019) 100, doi:http://dx.doi.org/10.1016/j.matlet.2018.12.135.
[127] M.F.R.P. Alves, C. dos Santos, C.M.F.A. Cossu, P.A. Suzuki, A.S. Ramos, E.C.T. Ramos, B.G. Simba, K. Strecker, Ceram. Int. 46 (2) (2020) 2344, doi:http://dx.doi.org/10.1016/j.ceramint.2019.09.225.
[128] J. Zhang, J. Zhang, G. Xiao, Z. Chen, M. Yi, Y. Zhang, C. Xu, Ceram. Int. 46 (3) (2020) 3550, doi:http://dx.doi.org/10.1016/j.ceramint.2019.10.072.
[129] J. Qiao, Y. Wen, Ceram. Int. 46 (1) (2020) 678, doi:http://dx.doi.org/10.1016/j.ceramint.2019.09.020.
[130] W. Chen, Z. Wang, X. Liu, J. Jia, Y. Hua, Tribol. Int. 141 (2020)105902, doi:http://dx.doi.org/10.1016/j.triboint.2019.105902.
[131] K. Kwatek, W. Ślubowska, J. Trébosc, O. Lafon, J.L. Nowiński, J. Eur. Ceram. Soc. 40 (1) (2020) 85, doi:http://dx.doi.org/10.1016/j.jeurceramsoc.2019.08.032.
[132] L. Huang, S. Ding, X. Yan, T. Song, Y. Zhang, J. Alloys Compd. 820 (2020)153100, doi:http://dx.doi.org/10.1016/j.jallcom.2019.153100.
[133] L. Wang, W. Kang, P. Gao, X. Liu, E.V. Rebrov, Ceram. Int. (2019), doi:http://dx.doi.org/10.1016/j.ceramint.2019.12.052 In Press.
[134] Y. Yuan, Z. Li, L. Cao, B. Tang, S. Zhang, Ceram. Int. 45 (13) (2019) 16569, doi:http://dx.doi.org/10.1016/j.ceramint.2019.05.194.
[135] M.T. Sebastian, H. Wang, H. Jantunen, Curr. Opin. Solid State Mater. Sci. 20 (3) (2016) 151, doi:http://dx.doi.org/10.1016/j.cossms.2016.02.004.
[136] P. Kumari, P. Tripathi, B. Sahu, S.P. Singh, O. Parkash, J. Phys. Chem. Solids 113 (2018) 177, doi:http://dx.doi.org/10.1016/j.jpcs.2017.10.028.
[137] S. Nakamura, MRS Bull. 22 (2) (1997) 29, doi:http://dx.doi.org/10.1557/S088376940003253X.
[138] A. Zerr, G. Miehe, G. Serghiou, M. Schwarz, E. Kroke, R. Riedel, H. Fuess, P. Kroll, R. Boehler, Nature 400 (1999) 340.
[139] V. Fuertes, M.J. Cabrera, J. Seores, D. Muñoz, J.F. Fernández, E. Enríquez, J. Eur. Ceram. Soc. 38 (7) (2018) 2759, doi:http://dx.doi.org/10.1016/j.jeurceramsoc.2018.02.009.
[140] J.E. Contreras, E.A. Rodríguez, Ceram. Int. 43 (12) (2017) 8545, doi:http://dx.doi.org/10.1016/j.ceramint.2017.04.105.
[141] R.A. Islam, Y.C. Chan, M.F. Islam, Mater. Sci. Eng. B 106 (2) (2004) 132, doi:http://dx.doi.org/10.1016/j.mseb.2003.09.005.
[142] J.X. Bi, C.F. Xing, Y.H. Zhang, C.H. Yang, H.T. Wu, J. Alloys Compd. 727 (2017) 123, doi:http://dx.doi.org/10.1016/j.jallcom.2017.08.110.
[143] I.M. Reaney, D. Iddles, J. Am. Ceram. Soc. 89 (2006) 2063, doi:http://dx.doi.org/10.1111/j.1551-2916.2006.01025.x.
[144] J.G. Korvink, W. Andrew, MEMS: A Practical Guide to Design, Analysis, and Applications, William Andrew, 2006.
[145] L.-A. Liew, Polymer-Derived Silicon Carbonitride as a New Technology for Microelectromechanical Systems, (2002) .
[146] R. Harshe, C. Balan, R. Riedel, J. Eur. Ceram. Soc. 24 (12) (2004) 3471, doi:http://dx.doi.org/10.1016/j.jeurceramsoc.2003.10.016.
[147] N. Szabo, C. Lee, J. Trimboli, O. Figueroa, R. Ramamoorthy, S. Midlam-Mohler, A. Soliman, H. Verweij, P. Dutta, S. Akbar, J. Mater. Sci. 38 (21) (2003) 4239, doi:http://dx.doi.org/10.1023/A:1026314511458.
[148] R. Raj, J. Am. Ceram. Soc. 76 (9) (1993) 2147, doi:http://dx.doi.org/10.1111/j.1151-2916.1993.tb07750.x.
[149] N.S. Jacobson, J. Am. Ceram. Soc. 76 (1) (1993) 3, doi:http://dx.doi.org/10.1111/j.1151-2916.1993.tb03684.x.
[150] E.J. Opila, R.E. Hann Jr, J. Am. Ceram. Soc. 80 (1) (1997) 197, doi:http://dx.doi.org/10.1111/j.1151-2916.1997.tb02810.x.
[151] K.N. Lee, Surf. Coatings Technol. 133–134 (2000) 1, doi:http://dx.doi.org/10.1016/S0257-8972(00)00889-6.
[152] U. Chowdhry, A. Sleight, Annu. Rev. Mater. Sci. 17 (2003) 323, doi:http://dx.doi.org/10.1146/annurev.ms.17.080187.001543.
[153] K.M. Lee, Z. Cai, J. Griggs, L. Guiatas, D.J. Lee, T. Okabe, J. Biomed, Mater. Res. B. Appl. Biomater. 68 (2004) 165, doi:http://dx.doi.org/10.1002/jbm.b.20017.
[154] L.A. Rocha, T.O. Ferreira, A.C. Monteiro, Key Eng. Mater. 230–232 (2002) 479 10.4028/www.scientific.net/KEM.230-232.479.
[155] N. Suansuwan, M. Swain, J. Dent. 31 (2003) 509, doi:http://dx.doi.org/10.1016/S0300-5712(03)00071-X.
[156] R.A.M. Receveur, F.W. Lindemans, N.F. de Rooij, J. Micromechanics Microengineering 17 (5) (2007) R50, doi:http://dx.doi.org/10.1088/0960-1317/17/5/r02.
[157] M.N. Rahaman, A. Yao, B. Bal, J. Garino, M.D. Ries, J. Am. Ceram. Soc. 90 (2007) 1965, doi:http://dx.doi.org/10.1111/j.1551-2916.2007.01725.x.
[158] C.J. Larmour, G. Bateman, D.R. Stirrups, Eur. J. Orthod. 28 (1) (2005) 74, doi:http://dx.doi.org/10.1093/ejo/cji072.
[159] H. Conrad, W.J. Seong, I. Pesun, J. Prosthet. Dent. 98 (2007) 389, doi:http://dx.doi.org/10.1016/S0022-3913(07)60124-3.
[160] D. Rekow, V.P. Thompson, J. Mater. Sci. Mater. Med. 18 (1) (2007) 47, doi:http://dx.doi.org/10.1007/s10856-006-0661-1.
[161] J.A. Fernie, R.A.L. Drew, K.M. Knowles, J.A. Fernie, R.A.L. Drew, K.M. Knowles, Int. Mater. Rev. 54 (5) (2009) 283, doi:http://dx.doi.org/10.1179/174328009X461078.
[162] G. Mustafa, K. Wyns, S. Janssens, A. Buekenhoudt, V. Meynen, Sep. Purif. Technol. 193 (2018) 29, doi:http://dx.doi.org/10.1016/j.seppur.2017.11.015.
[163] A. Oun, N. Tahri, S. Mahouche-Chergui, B. Carbonnier, S. Majumdar, S. Sarkar, G.C. Sahoo, R. Ben Amar, Sep. Purif. Technol. 188 (2017) 126, doi:http://dx.doi.org/10.1016/j.seppur.2017.07.005.
[164] S.M. Samaei, S. Gato-Trinidad, A. Altaee, Sep. Purif. Technol. 200 (2018) 198, doi:http://dx.doi.org/10.1016/j.seppur.2018.02.041.
[165] P. Geng, G. Chen, Sep. Purif. Technol. 185 (2017) 61, doi:http://dx.doi.org/10.1016/j.seppur.2017.05.023.
[166] M.R. Jamalludin, Z. Harun, S.K. Hubadillah, H. Basri, A.F. Ismail, M.H.D. Othman, M.F. Shohur, M.Z. Yunos, Chem. Eng. Res. Des. 114 (2016) 268, doi:http://dx.doi.org/10.1016/j.cherd.2016.08.023.
[167] J.-W. Wang, N.-X. Li, Z.-R. Li, J.-R. Wang, X. Xu, C.-S. Chen, Ceram. Int. 42 (7) (2016) 8949, doi:http://dx.doi.org/10.1016/j.ceramint.2016.02.153.
[168] B. Das, B. Chakrabarty, P. Barkakati, Ceram. Int. 42 (13) (2016) 14326, doi:http://dx.doi.org/10.1016/j.ceramint.2016.06.125.
[169] D.O. Obada, D. Dodoo-Arhin, M. Dauda, F.O. Anafi, A.S. Ahmed, O.A. Ajayi, Appl. Clay Sci. 132–133 (2016) 194, doi:http://dx.doi.org/10.1016/j.clay.2016.06.006.
[170] M. Peng, Y. Liu, H. Jiang, R. Chen, W. Xing, RSC Adv 6 (3) (2016) 2087, doi:http://dx.doi.org/10.1039/C5RA24150B.
[171] X. Mei, P.J. Quek, Z. Wang, H.Y. Ng, Bioresour. Technol. 240 (2017) 25, doi:http://dx.doi.org/10.1016/j.biortech.2017.02.052.
[172] B. Düppenbecker, M. Engelhart, P. Cornel, J. Membr. Sci. 537 (2017) 69, doi:http://dx.doi.org/10.1016/j.memsci.2017.05.018.
[173] Z. Yang, J. Cheng, C. Yang, B. Liang, Chin. J. Chem. Eng. 24 (10) (2016) 1375, doi:http://dx.doi.org/10.1016/j.cjche.2016.05.044.